Myocyte-Derived Hsp90 Modulates Collagen Upregulation via Biphasic Activation of STAT-3 in Fibroblasts during Cardiac Hypertrophy

Ritwik Datta,[a] Trisha Bansal,[a] Santanu Rana,[a] Kaberi Datta,[a] Ratul Datta Chaudhuri,[a] Mamta Chawla-Sarkar,[b] Sagartirtha Sarkar[a]

Genetics and Molecular Cardiology Laboratory, Department of Zoology, University of Calcutta, Kolkata, India[a]; Division of Virology, National Institute of Cholera and Enteric Diseases, Kolkata, India[b]

ABSTRACT Signal transducer and activator of transcription 3 (STAT-3)-mediated signaling in relation to upregulated collagen expression in fibroblasts during cardiac hypertrophy is well defined. Our recent findings have identified heat shock protein 90 (Hsp90) to be a critical modulator of fibrotic signaling in cardiac fibroblasts in this disease milieu. The present study was therefore intended to analyze the role of Hsp90 in the STAT-3-mediated collagen upregulation process. Our data revealed a significant difference between *in vivo* and *in vitro* results, pointing to a possible involvement of myocyte-fibroblast cross talk in this process. Cardiomyocyte-targeted knockdown of Hsp90 in rats (*Rattus norvegicus*) in which the renal artery was ligated showed downregulated collagen synthesis. Furthermore, the results obtained with cardiac fibroblasts conditioned with Hsp90-inhibited hypertrophied myocyte supernatant pointed toward cardiomyocytes' role in the regulation of collagen expression in fibroblasts during hypertrophy. Our study also revealed a novel signaling mechanism where myocyte-derived Hsp90 orchestrates not only p65-mediated interleukin-6 (IL-6) synthesis but also its release in exosomal vesicles. Such myocyte-derived exosomes and myocyte-secreted IL-6 are responsible in unison for the biphasic activation of STAT-3 signaling in cardiac fibroblasts that culminates in excess collagen synthesis, leading to severely compromised cardiac function during cardiac hypertrophy.

KEYWORDS cardiac hypertrophy, collagen, Hsp90, myocyte-fibroblast cross talk, STAT-3

Myocardial fibrosis is a hallmark of cardiac hypertrophy and a proposed substrate for heart failure (1, 2). The extracellular space is frequently the site for such abnormal accumulation of fibrillar collagen, accounting for myocardial stiffness and ventricular dysfunction during cardiac hypertrophy (3). The cardiac fibroblast is the principal cell type in the myocardium and synthesizes and secretes collagen in response to pressure-overload hypertrophy (4). A close relationship between angiotensin II (AngII) and profibrotic cytokines has been suggested, and several molecular signaling networks have been implicated in the progression of cardiac fibrosis (5, 6). A few reports have also shown that the role of myocytes in myocardial collagen production is mediated by myocyte-derived paracrine factors (7, 8). However, the precise mechanisms involving the role of different signaling intermediates in the regulation of collagen gene expression during cardiac hypertrophy have remained unsolved.

In an earlier report, we described the mechanism of interleukin-6 (IL-6)-mediated activation of the signal transducer and activator of transcription 3 (STAT-3) and consequent collagen synthesis in the hypertrophied rat heart (9). STAT-3 activation has also

been reported in the pressure-overloaded feline myocardium (10). AngII has been shown to act in concert with hyperglycemia to upregulate collagen synthesis in cardiac fibroblasts via a STAT-3-dependent mechanism (11). STAT-3 is now considered a multifaceted molecule initially found to be regulated by the IL-6–gp130 system (12). The activation of STAT-3 by the paracrine action of IL-6 has been extensively documented in different cell types (13–15). Such cytokine-mediated signal transduction by STATs has been found to involve a continuous signaling cycle (16), where Janus kinase (JAK) and tyrosine kinase 2 (Tyk-2) at the intracytoplasmic domain of the gp130 receptor regulate the phosphorylation of STAT-3 at tyrosine-705 (17, 18). The cytokine-induced activation of STAT-3 has also been associated with its decreased rate of nuclear exit, resulting in its retention at a higher level within the nucleus (19, 20). Another critical level of regulation of STAT-3 activity includes its interaction with the chaperone heat shock protein 90 (Hsp90) (21–23). Schoof et al. (24) have shown the central role of Hsp90 in JAK-STAT signaling during classical Hodgkin's lymphoma. IL-6-activated STAT-3 signaling has also been found to be sensitive to Hsp90 inhibition in multiple myeloma cells (25). However, until now there have been no reports describing the role of Hsp90 in STAT-3 activation during cardiac hypertrophy.

Our recent findings (26) as well as those of other groups have indicated that Hsp90 is a critical modulator of fibrosis via alteration of the TGFβ signaling pathway (27–30). To further develop this line of research, the present study was designed to look into the possible role of Hsp90 in STAT-3-mediated fibrotic signaling during cardiac hypertrophy and associated fibrosis.

A significant difference between *in vivo* and *in vitro* results in a pilot study hinted toward a possible involvement of cellular cross talk. This study aims to determine how Hsp90 of the myocytes acts as a node of control over collagen biosynthesis in fibroblasts via regulation of the biphasic activation of STAT-3.

RESULTS

Differential activation of STAT-3 *in vitro* and *in vivo* during Hsp90 inhibition. The ratio of phosphorylated STAT-3/total STAT-3 in Hsp90-inhibited hypertrophied fibroblasts remained unaltered from that in AngII-treated cells (Fig. 1a and b). Hypertrophied myocytes also showed an insignificant change in the phosphorylation status of STAT-3 during Hsp90 inhibition compared with that for AngII-treated cells (Fig. 1c and d). Treatment with Hsp90 small interfering (siRNA) yielded similar results in both cell types, as observed by the chemical inhibition of Hsp90 (Fig. 1a to d). Successful knockdown of Hsp90 during hypertrophy in both cell types was confirmed by immunoblotting with anti-Hsp90 antibody (Fig. 1e).

However, Hsp90 inhibition *in vivo* showed significant downregulation (2.46-fold ± 0.10-fold) in the level of phosphorylation of STAT-3 Y705 and STAT-3 S727 compared to that in rat hearts in which the renal artery was ligated (Fig. 2a, left, and b). Myocyte-specific knockdown of Hsp90 expression during hypertrophy *in vivo* also significantly decreased the ratio of phosphorylated STAT-3/total STAT-3 (2.13-fold ± 0.10-fold and 1.88-fold ± 0.17-fold for STAT-3 Y705 and STAT-3 S727, respectively) compared to that in ligated rat hearts (Fig. 2a, right, and b). Successful knockdown of Hsp90 expression in the myocardium during hypertrophy was confirmed by immunoblotting with anti-Hsp90 antibody (Fig. 2e).

Moreover, myocyte-fibroblast coculture *in vitro* revealed the significant downregulation of phosphorylation of STAT-3 in fibroblasts during Hsp90 inhibition in myocytes. Fibroblasts incubated with Hsp90 siRNA and inhibitor-treated hypertrophied myocyte-conditioned medium (MCM) showed 5.11-fold ± 0.27-fold and 3.38-fold ± 0.21-fold downregulation in STAT-3 Y705 and STAT-3 S727 phosphorylation levels, respectively, compared to those for fibroblasts incubated with the AngII-treated myocyte culture supernatant (Fig. 2c and d). Similar results were observed when fibroblasts were cocultured with Hsp90 siRNA-treated hypertrophied myocytes grown on inserts (data not shown).
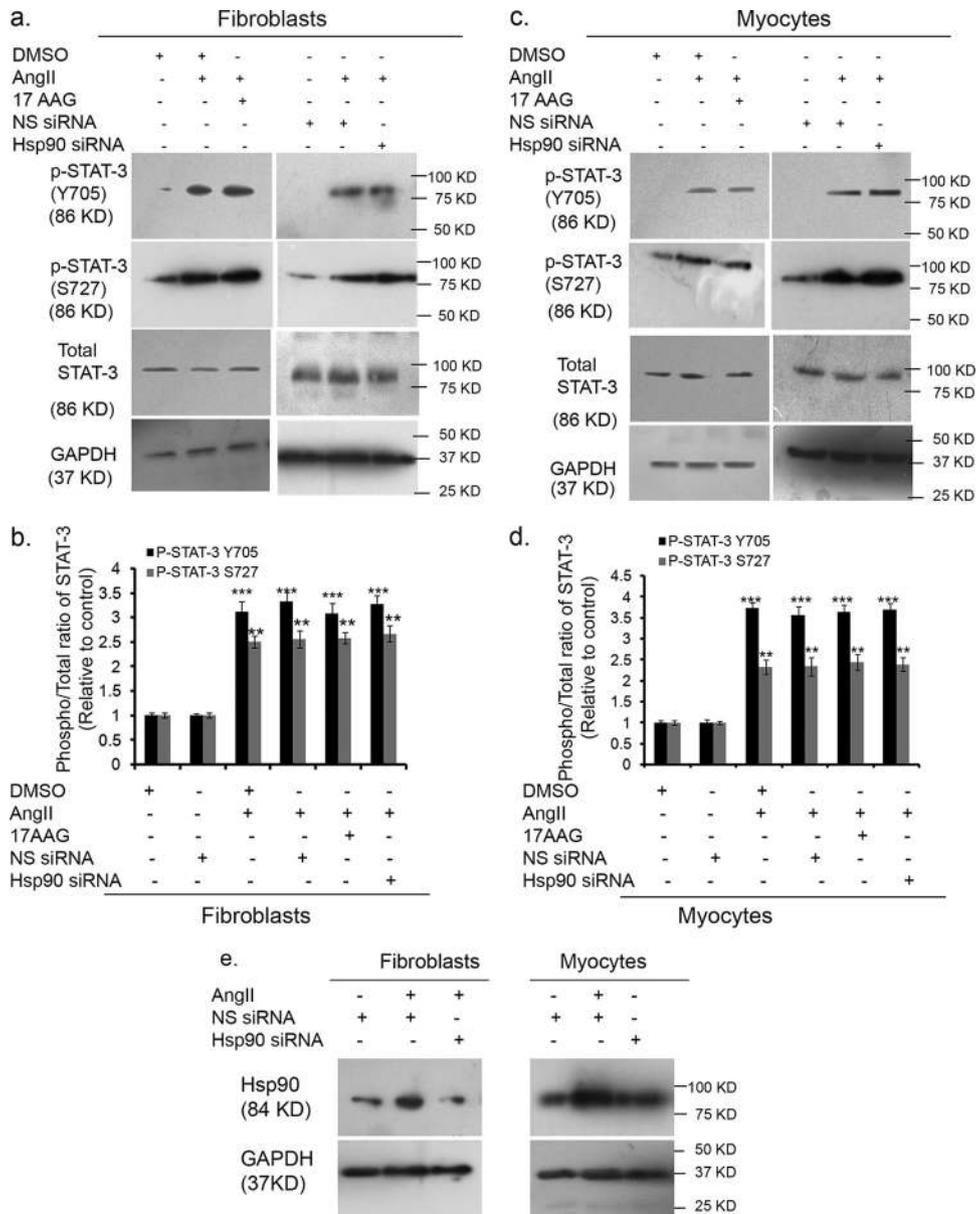
FIG 1 Hsp90 inhibition during hypertrophy has no effect on STAT-3 phosphorylation either in fibroblasts or in myocytes alone. (a) Western blots showing the unchanged ratio of phosphorylated-STAT-3 (p-STAT-3)/total STAT-3 in hypertrophied fibroblasts upon treatment with either 17-AAG or Hsp90 siRNA. GAPDH was used as a loading control. Results are expressed as the mean ± SE from three independent experiments (n = 10 for each group). (b) Graphical representation showing the unchanged ratio of phosphorylated STAT-3/total STAT-3 in hypertrophied fibroblasts upon treatment with either 17-AAG or Hsp90 siRNA. Results are expressed as the mean ± SE from three independent experiments (n = 10 for each group). **, P < 0.01 with respect to the respective control; ***, P < 0.001 with respect to the respective control. (c) Western blots showing the ratio of phosphorylated STAT-3/total STAT-3 in hypertrophied cardiomyocytes upon treatment with either 17-AAG or Hsp90 siRNA. GAPDH was used as a loading control. Results are expressed as the mean ± SE from three independent experiments (n = 10 for each group). (d) Graphical representation showing the unchanged ratio of phosphorylated STAT-3/total STAT-3 in hypertrophied cardiomyocytes upon treatment with either 17-AAG or Hsp90 siRNA. Results are expressed as the mean ± SE from three independent experiments (n = 10 for each group). **, P < 0.01 with respect to the respective control; ***, P < 0.001 with respect to the respective control. (e) Western blots confirming the siRNA-mediated knockdown of Hsp90 expression during hypertrophy in different cell types. GAPDH was used as a loading control (n = 10 for each group).

Consistent with the reduced level of STAT-3 phosphorylation, collagen gene expression was significantly downregulated in fibroblasts incubated with Hsp90 siRNA-treated hypertrophied MCM (2.66-fold ± 0.02-fold for *Col-1* and 2.13-fold ± 0.04-fold for *Col-3*) compared to that in fibroblasts incubated with AngII-treated MCM (Fig. 3a, right).
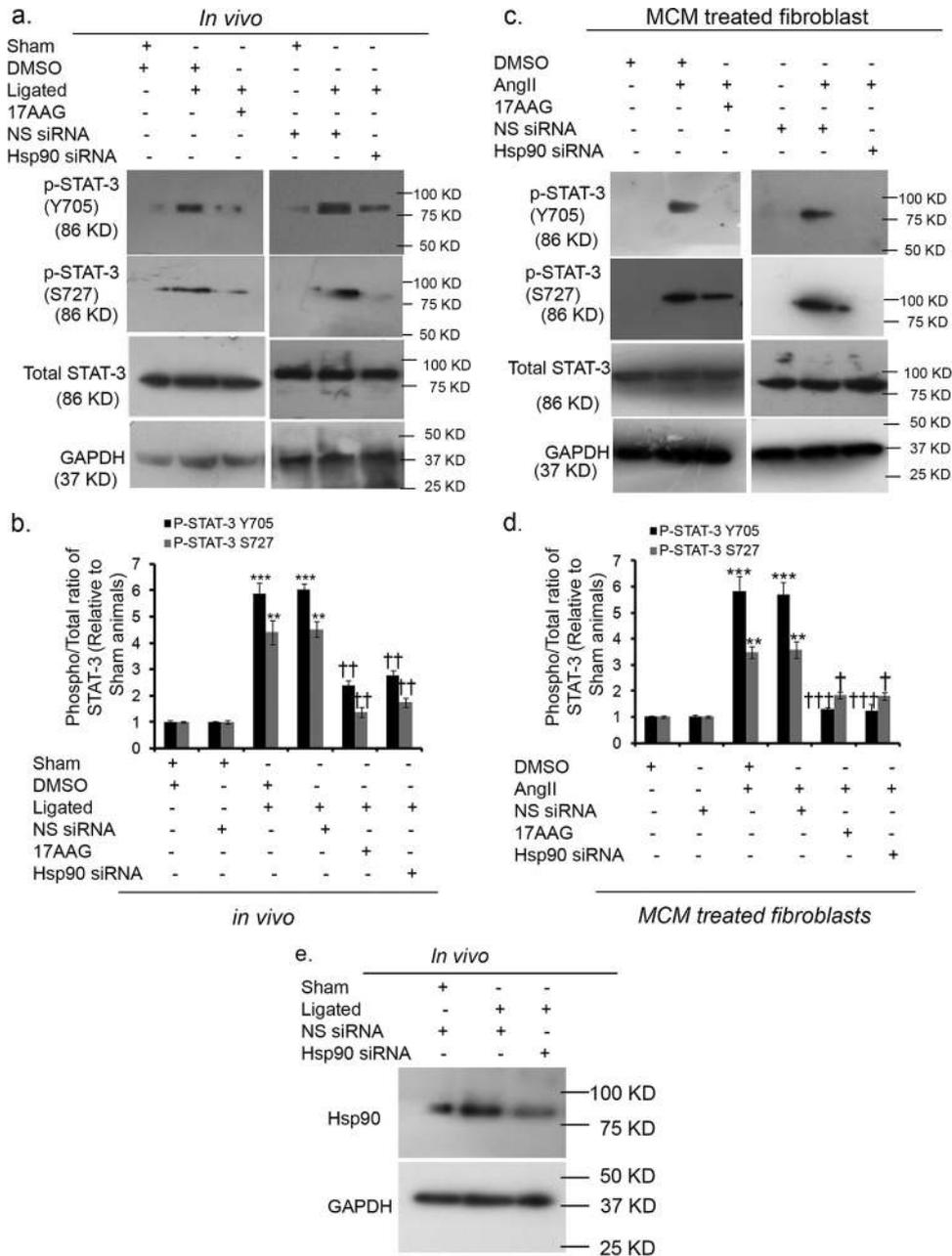
FIG 2 Hsp90 inhibition in myocytes abrogates STAT-3 phosphorylation in myocyte-conditioned fibroblasts. (a) Western blots showing the significantly reduced phosphorylation of STAT-3 in 17-AAG-treated hypertrophied rat hearts compared to ligated rat hearts *in vivo*. GAPDH was used as a loading control ($n = 10$ for each group). Myocyte-specific knockdown of Hsp90 by CMC-peptide-conjugated Hsp90 siRNA treatment during hypertrophy also significantly reduced the ratio of phosphorylated STAT-3/total STAT-3 compared to that for hypertrophied rat heart subjected to treatment with CMC-peptide-conjugated NS siRNA. GAPDH was used as a loading control ($n = 10$ for each group). (b) Graphical representation showing the downregulated phosphorylation of STAT-3 during Hsp90 inhibition in hypertrophied hearts. Results are expressed as the mean $\pm$ SE from three independent experiments ($n = 10$ for each group). **, $P < 0.01$ with respect to the respective control rats that underwent a sham operation; ***, $P < 0.001$ with respect to the respective control rats that underwent a sham operation; ††, $P < 0.01$ with respect to the respective hypertrophy group. (c) Western blots showing significant downregulation of phosphorylated STAT-3 in fibroblasts conditioned with 17-AAG-treated hypertrophied MCM compared to fibroblasts conditioned with AngII-treated myocyte supernatant. The results observed in fibroblasts conditioned with Hsp90 siRNA-treated hypertrophied MCM were similar to those observed in fibroblasts conditioned with NS siRNA-treated hypertrophied MCM. GAPDH was used as a loading control. Results are expressed as the mean $\pm$ SE from three independent experiments ($n = 10$ for each group). (d) Graphical representation showing the significant downregulation of phosphorylated STAT-3 in MCM-treated fibroblasts during Hsp90 inhibition in myocytes. Results are expressed as the mean $\pm$ SE from three independent experiments ($n = 10$ for each group). ***, $P < 0.001$ with respect to the respective controls; **, $P < 0.01$ with respect to the respective controls; †††, $P < 0.001$ with respect to the respective hypertrophied MCM-treated fibroblasts; †, $P < 0.05$ with respect to the respective hypertrophied

(Continued on next page)

A hydroxyproline assay also revealed a significant reduction in the amount of secreted collagen (1.46-fold $\pm$ 0.05-fold) in these fibroblasts (Fig. 3b).

Myocyte-targeted Hsp90 knockdown during hypertrophy *in vivo* showed a significant downregulation in collagen gene expression (1.90-fold $\pm$ 0.02-fold and 2.50-fold $\pm$ 0.16-fold for *Col-1* and *Col-3*, respectively) as well as the left ventricular collagen content (1.39-fold $\pm$ 0.04-fold) compared to those for hypertrophy samples (Fig. 3a, left, and c). Histological analysis with Masson's trichrome staining also revealed a significantly reduced collagen volume fraction (CVF) in rat hearts in which the renal artery was ligated and that were treated with carboxy methyl chitosan (CMC) peptide-conjugated Hsp90 siRNA compared to that in the hypertrophy group (2.86-fold $\pm$ 0.29-fold compared with that in the hypertrophy group) (Fig. 3d). Myocyte-specific Hsp90 knockdown in rats in which the renal artery was ligated also resulted in improved cardiac function, as evidenced by a decreased left ventricular diastolic dimension (LVDD; 5.18 $\pm$ 0.12 mm), and restored the percentage of fractional shortening (FS; 40.92% $\pm$ 0.65%) compared to the LVDD and FS in rats in which the renal artery was ligated (LVDD, 5.93 $\pm$ 0.06 mm; FS, 33.25% $\pm$ 1.11%) (Fig. 3e).

Activation of STAT-3 in fibroblasts depends on IL-6 secreted from myocytes. Hsp90 siRNA-treated hypertrophied myocyte supernatants showed significantly decreased amounts of secreted IL-6 (3.38-fold $\pm$ 0.20-fold) compared to that for nonspecific (NS) siRNA-treated hypertrophied myocyte supernatants, as evident from an IL-6 enzyme-linked immunosorbent assay (ELISA) (Fig. 4a). Myocyte-derived IL-11 or leukemia inhibitory factor (LIF) was found in trace amounts in the culture supernatants compared to the amount of IL-6 that was found. The amount of IL-11 or LIF from culture supernatants of both hypertrophied and Hsp90 siRNA-treated myocytes also was not significantly altered compared to that from culture supernatants of untreated myocytes (data not shown). Immunoblot analysis revealed downregulated IL-6 expression during Hsp90 knockdown in AngII-treated myocytes and in ligated heart samples (3.26-fold $\pm$ 0.24-fold *in vitro* and 2.07-fold $\pm$ 0.04-fold *in vivo*) compared to that in the respective NS siRNA-treated hypertrophy samples (Fig. 4b). An immunofluorescence study using IL-6 antibody in ventricular tissue sections *in vivo* reconfirmed these data (Fig. 4c).

Fibroblasts incubated with IL-6-neutralized hypertrophied myocyte supernatant significantly downregulated the expression of phosphorylated STAT-3 (3.70-fold $\pm$ 0.51-fold and 2.83-fold $\pm$ 0.23-fold for STAT-3 Y705 and STAT-3 S727, respectively) compared to that in fibroblasts conditioned only with hypertrophied myocyte supernatant (Fig. 5a). Successful IL-6 neutralization was again confirmed by the IL-6 ELISA (data not shown). IL-6-neutralized myocyte supernatant-conditioned fibroblasts also showed reduced expression of collagen genes (2.35-fold $\pm$ 0.11-fold and 2.12-fold $\pm$ 0.13-fold regression for *Col-1* and *Col-3*, respectively) compared to that in AngII-treated myocyte-conditioned fibroblasts (Fig. 5b).

IL-6 synthesis in myocytes is regulated by Hsp90. Western blot analyses revealed the significant downregulation of total and nuclear p65 and C/EBPβ in Hsp90 siRNA-treated hypertrophy samples compared to that in the NS siRNA-treated hypertrophy groups both *in vitro* and *in vivo* (Fig. 6a and b).

p65 siRNA treatment of hypertrophied myocytes also resulted in the significant downregulation of IL-6 activity (2.41-fold $\pm$ 0.20-fold) compared to that in AngII-treated myocytes (Fig. 6c). However, C/EBPβ siRNA treatment of hypertrophied myocytes had no significant effect on IL-6 activity (Fig. 6c).

Fibroblasts conditioned with p65 siRNA-treated hypertrophied myocytes showed significantly reduced levels of expression of phosphorylated STAT-3 (2.80-fold $\pm$ 0.07-fold for STAT-3 Y705 and 1.69-fold $\pm$ 0.06-fold for STAT-3 S727) as well as the collagen genes (1.47-fold $\pm$ 0.13-fold for *Col-1* and 1.84-fold $\pm$ 0.17-fold for *Col-3*) compared to

FIG 2 Legend (Continued)
MCM-treated fibroblasts. (e) Western blot analysis revealed the successful knockdown of Hsp90 expression in CMC-peptide-conjugated Hsp90 siRNA-treated hypertrophied hearts but not the CMC-peptide-conjugated NS siRNA-treated hypertrophy samples *in vivo*. GAPDH was used as a loading control ($n = 10$ for each group).
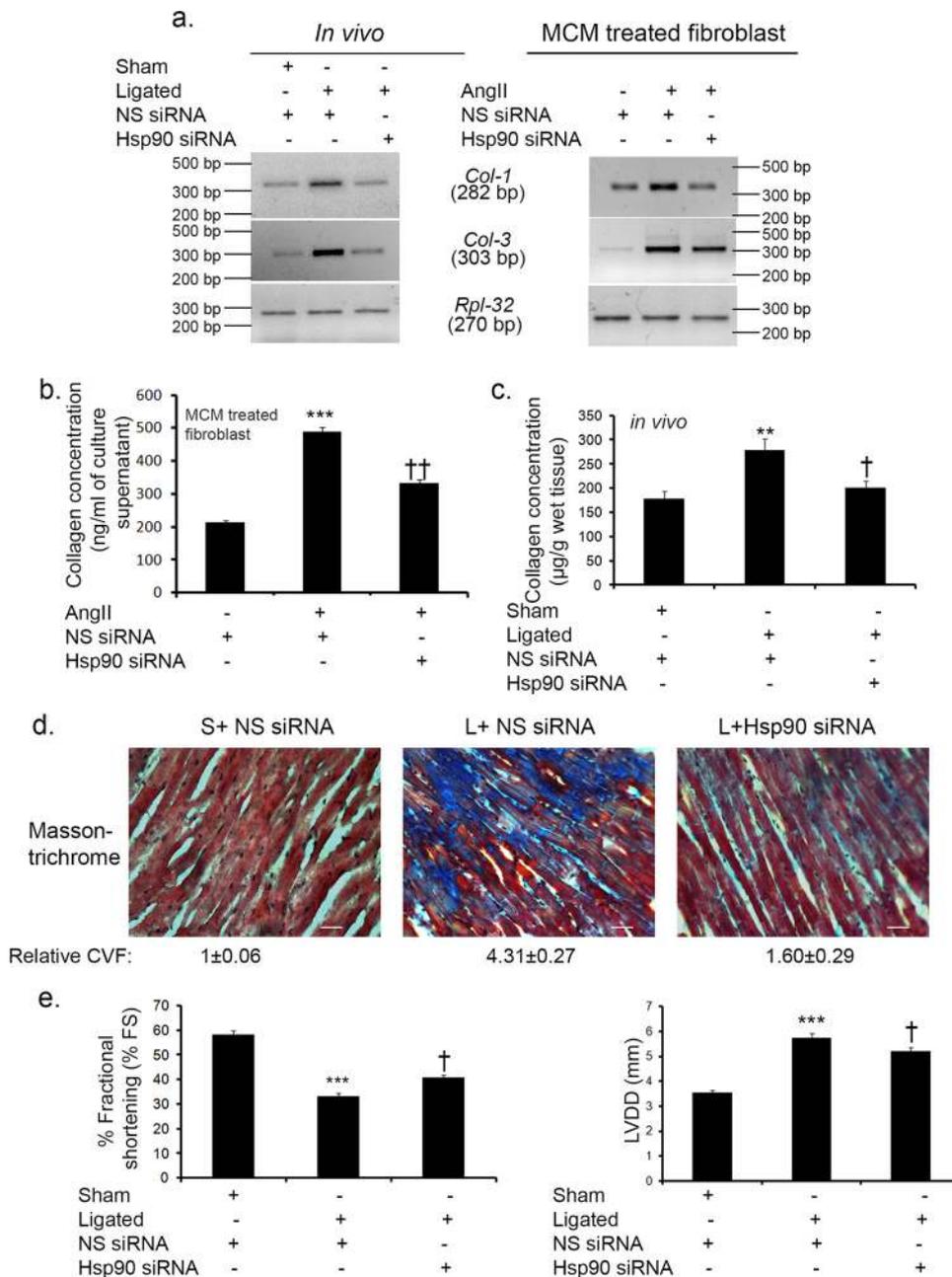
FIG 3 Hsp90 inhibition in hypertrophied myocytes regresses fibrosis and restores cardiac function. (a) Cardiomyocyte-specific Hsp90 siRNA treatment in rats in which the renal artery was ligated showing the significant downregulation of collagen gene expression compared to that in NS siRNA-treated rat hearts in which the renal artery was ligated *in vivo*, as revealed by RT-PCR. A significant reduction in collagen gene expression was also observed in fibroblasts conditioned with Hsp90 siRNA-treated hypertrophied MCM compared to that in fibroblasts conditioned with NS siRNA-treated hypertrophied MCM *in vitro*. Rpl-32 was used as a loading control ($n = 10$ for each group). (b) A hydroxyproline assay showed a significant reduction in the secreted collagen content from fibroblasts conditioned with Hsp90 siRNA-treated hypertrophied MCM (333.33 ± 9.21 ng/ml) compared to that in fibroblasts conditioned with NS siRNA-treated hypertrophied MCM (488 ± 14.46 ng/ml). Results are expressed as the mean $\pm$ SE from three independent experiments ($n = 10$ for each group). (c) A hydroxyproline assay showed a significant reduction in the total left ventricular collagen content in CMC-peptide-conjugated Hsp90 siRNA-treated hypertrophied rat hearts (278.5 ± 13.5 μg/g) compared to that in CMC-peptide-conjugated NS siRNA-treated rats in which the renal artery was ligated (201.3 ± 13.6) *in vivo*. (d) Masson's trichrome staining showing a significant reduction in the collagen volume fraction (CVF) in CMC-peptide-conjugated Hsp90 siRNA-treated hypertrophied rat hearts compared to CMC-peptide-conjugated NS siRNA-treated hypertrophy samples *in vivo*. Results are expressed as the mean $\pm$ SE from three independent experiments ($n = 10$ for each group). S+ NS siRNA, hearts from control rats that underwent a sham operation treated with CMC-peptide-conjugated NS siRNA; L+ NS siRNA, hearts from rats in which the renal artery was ligated treated with CMC-peptide-conjugated NS siRNA; L+ Hsp90 siRNA, hearts from rats in which the renal artery was ligated treated with CMC-peptide-conjugated

(Continued on next page)

those for hypertrophied MCM-treated fibroblasts (Fig. 6d and e). However, C/EBPβ siRNA treatment of hypertrophied myocytes showed no significant effect on either STAT-3 phosphorylation or subsequent collagen expression in similar MCM-treated fibroblasts (Fig. 6d and e).

The transcriptional activity of p65 in isolated myocytes was then assessed by a luciferase assay. p65 activity was significantly downregulated (4.34-fold $\pm$ 0.20-fold) in Hsp90 siRNA-treated hypertrophied myocytes compared to the level of regulation in NS siRNA-treated AngII-infused cells *in vitro* (Fig. 7a). The immunofluorescence study also showed a significant reduction in the amount of phospho-p65-positive nuclei in Hsp90 siRNA-treated hypertrophied myocytes compared to that in NS siRNA-treated hypertrophied cells (76% $\pm$ 3.43% versus 43% $\pm$ 2.71%) (Fig. 7b).

Hsp90-mediated regulation of p65 in myocytes. The expression status of the proteins upstream of p65 was assessed by Western blot analyses both *in vitro* and *in vivo* and revealed markedly reduced levels of expression of IκB kinase (IKKβ) (2.03-fold $\pm$ 0.06-fold regression *in vitro* and 2.58-fold $\pm$ 0.21-fold regression *in vivo*) and phospho-IκB (5.27-fold $\pm$ 0.18-fold regression *in vitro* and 6.05-fold $\pm$ 0.18-fold regression *in vivo*) in Hsp90 siRNA-treated hypertrophy samples compared to those in hypertrophy samples alone (Fig. 7c). The binding of Hsp90 to IKKβ studied in 17-allylamino-17-demethoxygeldanamycin (17-AAG)-treated hypertrophied myocytes revealed a significant reduction in the amount of Hsp90-bound IKKβ (2.48-fold $\pm$ 0.19-fold) compared to that in AngII-treated cells, as shown by coimmunoprecipitation experiments (Fig. 7d). The direct binding efficiency of the Hsp90 N-terminal ATPase domain to IKKβ was further assessed by fluorescence recovery after photobleaching (FRAP) analysis, which revealed a significant fluorescence resonance energy transfer (FRET) efficiency (27.3% $\pm$ 2.88%) between the two proteins (Fig. 8a). Treatment of cells with 17-AAG reduced the FRET efficiency to 12% $\pm$ 1.3%, thus confirming the specificity of the interaction.

Immunoprecipitation with anti-Hsp90 antibody followed by Western blotting with anti-Cdc37 antibody revealed a significantly higher level of association of Cdc37 with Hsp90 in AngII-treated myocytes compared to that for the control, which was significantly blocked by treatment with celastrol (2.14-fold $\pm$ 0.16-fold) (Fig. 8b). Blocking of such an interaction between Hsp90 and Cdc37 with celastrol in hypertrophied myocytes significantly reduced the level of binding of IKKβ to Hsp90 (1.46 $\pm$ 0.07-fold) compared to that in hypertrophied myocytes alone (Fig. 8b). However, celastrol treatment of hypertrophied myocytes did not alter the binding of IKKβ to Cdc37 (Fig. 8c).

Stabilization of IKKβ by the Hsp90/Cdc37 complex in myocytes is crucial for induction of collagen from fibroblasts. (i) The absence of Hsp90/Cdc37 activity degrades IKKβ via the ubiquitin proteasome machinery. The expression level of IKKβ in hypertrophied myocytes was quantified after simultaneous pretreatment of these myocytes with either 17-AAG and MG132 or celastrol and MG132. MG132 treatment significantly rescued the regressed expression levels of IKKβ in either 17-AAG-treated hypertrophied myocytes (1.71-fold $\pm$ 0.16-fold) or celastrol-treated hypertrophied myocytes (1.82-fold $\pm$ 0.14-fold), indicating the compromised stability of IKKβ in the absence of its interaction with Hsp90 (Fig. 9a).

Immunoprecipitation of proteins with IKKβ followed by immunoblotting with an antiubiquitin antibody showed a significantly higher level of polyubiquitination of IKKβ, as evident in either 17-AAG- or celastrol-treated hypertrophied cells under conditions of proteasomal inhibition (1.92-fold $\pm$ 0.09-fold and 3.48-fold $\pm$ 0.34-fold, respectively) compared with that in MG132-treated hypertrophied myocytes, suggesting the induc-

FIG 3 Legend (Continued)
Hsp90 siRNA. Bars, 50 μm. Magnification, $\times$40. (e) The restored FS (in percent) and decreased LVDD in CMC-peptide-conjugated Hsp90 siRNA-treated hypertrophied rat hearts compared to those in CMC-peptide-conjugated NS siRNA-treated rat hearts in which the renal artery was ligated. Results are expressed as the mean $\pm$ SE from three independent experiments (n = 10 for each group). ***, $P < 0.001$ with respect to the control that underwent a sham operation; †, $P < 0.05$ with respect to the NS siRNA-treated ligated rat heart.
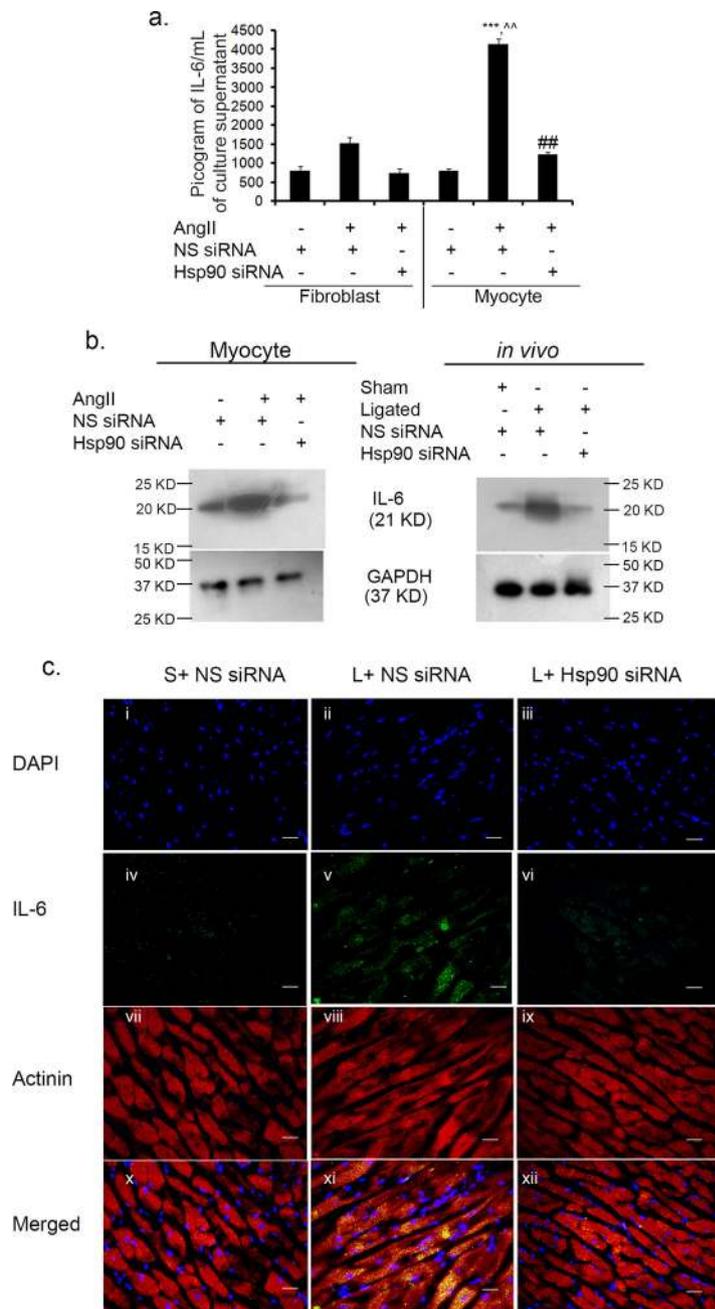
FIG 4 Hsp90 inhibition downregulates IL-6 expression during hypertrophy. (a) Graphical representation of results of IL-6 ELISA, which showed significant downregulation of the concentration of active IL-6 in supernatants of Hsp90 siRNA-treated hypertrophied myocytes compared to that in supernatants of AngII-treated myocytes. AngII-induced IL-6 secretion is significantly higher in myocytes than fibroblasts. Results were analyzed by one-way ANOVA followed by Tukey's *post hoc* test and expressed as the mean $\pm$ SE from three independent experiments ($n = 5$ for each group). ***, $P < 0.001$ with respect to control myocytes; ##, $P < 0.01$ with respect to hypertrophied myocytes; ^^, $P < 0.01$ with respect to AngII-treated fibroblasts. (b) Western blot analysis showing the significant downregulation of IL-6 expression in Hsp90 siRNA-treated hypertrophy samples compared to the respective hypertrophy groups both *in vitro* (myocyte) and *in vivo*. Results are expressed as the mean $\pm$ SE from three independent experiments ($n = 10$ for each group). (c) Immunofluorescence study showing reduced expression of IL-6 in CMC-peptide-conjugated Hsp90 siRNA-treated hypertrophied rat hearts compared to that in CMC-peptide-conjugated NS siRNA-treated hypertrophy samples. (i to iii) DAPI staining; (iv to vi) IL-6 expression; (vii to ix) actinin expression; (ix to xii) merged images ($n = 5$ for each group). S+ NS siRNA, hearts from control rats that underwent a sham operation treated with CMC-peptide-conjugated NS siRNA; L+ NS siRNA, hearts from rats in which the renal artery was ligated treated with CMC-peptide-conjugated NS siRNA; L+ Hsp90 siRNA, hearts from rats in which the renal artery was ligated treated with CMC-peptide-conjugated Hsp90 siRNA. Bars, 50 μm. Magnification, $\times$40.
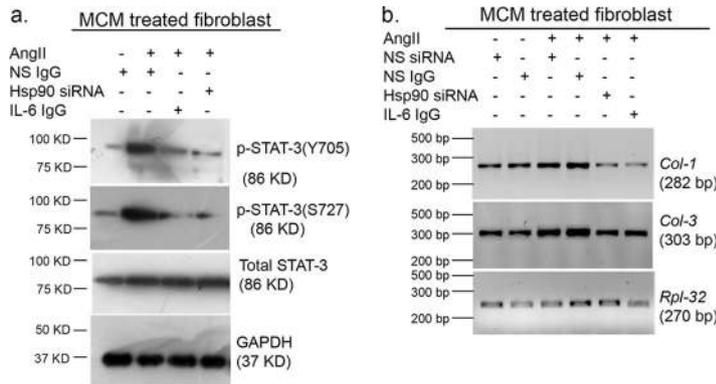
FIG 5 Hsp90-mediated regulation of IL-6 in myocytes is crucial for STAT-3-driven collagen gene expression in fibroblasts during cardiac hypertrophy. (a) Western blot analysis revealed the significant downregulation of phosphorylated STAT-3 in fibroblasts conditioned with IL-6-neutralized hypertrophied MCM compared to fibroblasts conditioned with hypertrophied MCM. GAPDH was used as an internal loading control ($n = 10$ for each group). Control and hypertrophied myocytes treated with either NS IgG (used as an isotype control) or NS siRNA yielded similar results. (b) RT-PCR analysis showing significantly reduced levels of collagen gene expression in fibroblasts conditioned with IL-6-neutralized hypertrophied MCM compared to fibroblasts conditioned with NS IgG-treated hypertrophied MCM ($n = 10$ for each group). Rpl-32 was used as an internal loading control.

tion of ubiquitination of IKKβ by 17-AAG and celastrol treatment during myocyte hypertrophy (Fig. 9b).

(ii) Proteasomal inhibition in 17-AAG- or celastrol-treated hypertrophied myocytes partially restores collagen expression in fibroblasts. Conditioning of fibroblasts with proteasome-inhibited 17-AAG- or celastrol-treated hypertrophied myocyte supernatant restored collagen gene expression (1.81-fold ± 0.12-fold and 1.66-fold ± 0.11-fold, respectively, for Col-1; 1.86-fold ± 0.08-fold and 1.74-fold ± 0.05-fold, respectively, for Col-3), compared to groups where fibroblasts were conditioned with either 17-AAG- or celastrol-treated hypertrophied myocyte supernatant (Fig. 9c).

Myocyte-derived exosomes containing Hsp90 and IL-6 transmigrate to fibroblasts during hypertrophy. The exosomal protein concentration was significantly higher in AngII-treated myocyte supernatant (2.31-fold ± 0.11-fold) than the control myocyte supernatant, in which the exosomal protein content was again downregulated during Hsp90 siRNA treatment in hypertrophied myocytes (1.62-fold ± 0.05-fold), as revealed by a micro-bicinchoninic acid (micro-BCA) protein estimation assay (Fig. 10a). Expression of the exosomal marker CD63 in myocytes revealed an altered pattern of CD63 glycosylation in Hsp90 siRNA-treated hypertrophied myocytes compared to that in NS siRNA-treated hypertrophied cells (Fig. 10b). Coimmunoprecipitation analysis showed an association of Hsp90 with a specific glycosylated form of CD63 (molecular mass, between 40 and 50 kDa) in AngII-treated myocytes. Such an interaction was completely abolished when hypertrophied myocytes were treated with Hsp90 siRNA (Fig. 10b). A significant increase in the expression of Hsp90 and IL-6 in myocyte-derived exosomes was observed by AngII treatment; the expression was significantly reduced in the supernatant of Hsp90 siRNA-treated hypertrophied myocyte-derived exosomes (Fig. 10c).

Furthermore, Western blot analysis of exosomal fractions revealed the presence of Hsp90 in the exosomal membrane after carbonate treatment. Carbonate treatment followed by proteinase K treatment removed Hsp90. However, IL-6 was present in exosome isolates treated only with proteinase K (Fig. 10d).

To confirm the transmigration of the same exosomes from myocytes inside fibroblasts during hypertrophy, CD63 was overexpressed in myocytes, and culture supernatants from each treatment group were then transferred to fibroblast cultures. Fibroblasts treated with hypertrophied MCM showed a significantly higher rate of positivity for green fluorescent protein (GFP)-tagged CD63 (CD63-GFP) (32% ± 5%) than fibro-
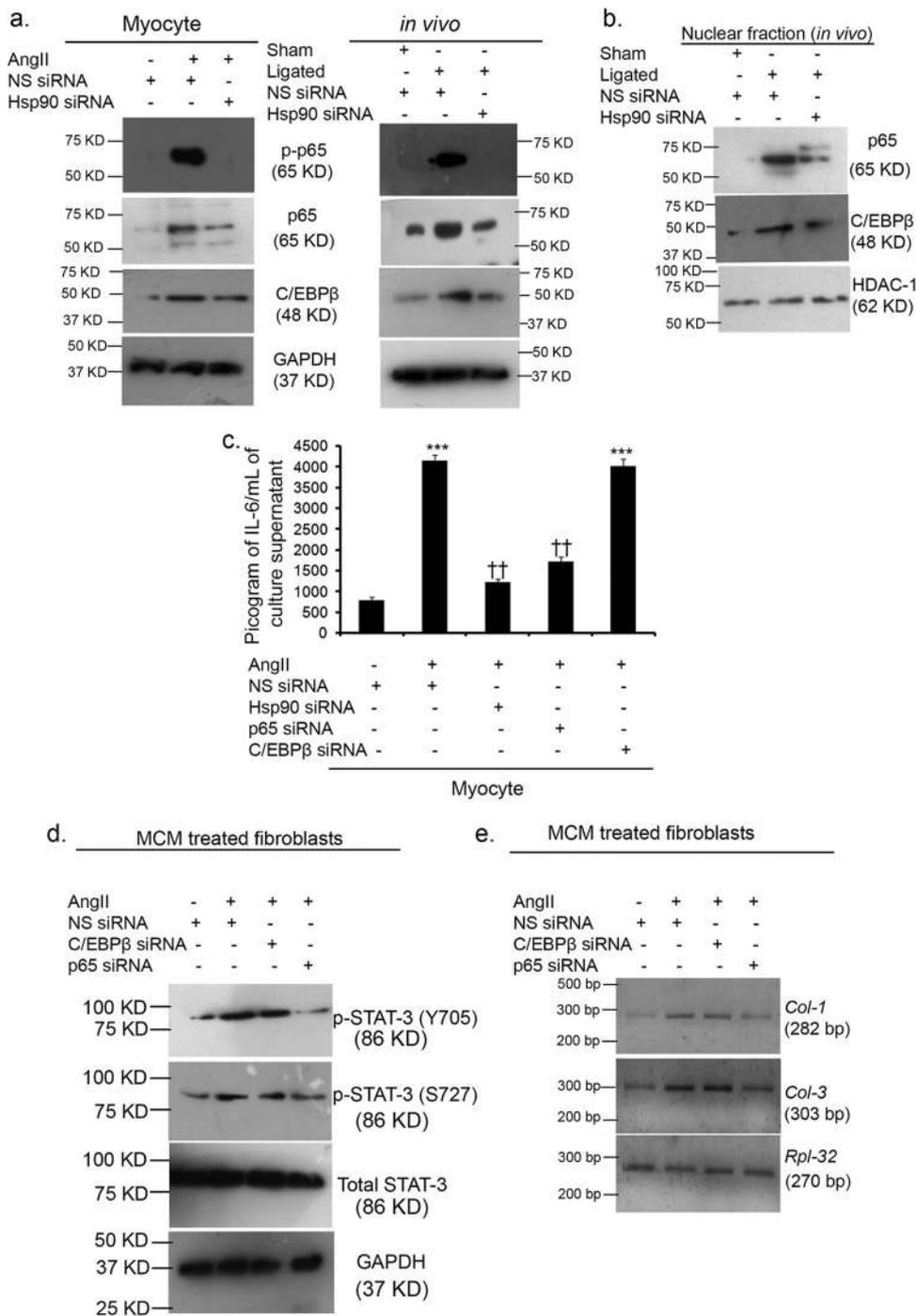
FIG 6 Hsp90 inhibition in hypertrophied myocytes alters IL-6 expression and consequent fibrosis predominantly via p65. (a) Western blot analysis revealed the significant downregulation of p65 and C/EBPβ expression upon Hsp90 siRNA treatment during hypertrophy compared to that in the respective hypertrophy samples in vitro and in vivo (n = 10 for each group). GAPDH was used as an internal loading control. (b) Western blot analysis revealed the significant downregulation of nuclear expression of p65 and C/EBPβ upon cardiomyocyte-specific knockdown of Hsp90 in hypertrophied myocardium compared to that in rat hearts in which the renal artery was ligated in vivo. HDAC-1 was used as a loading control (n = 5 for each group). (c) Graphical representation of the IL-6 ELISA results showing a significant reduction in the amount of secreted IL-6 in p65 siRNA-treated hypertrophied myocytes (1,723.6 ± 117.64 pg/ml) compared to that in NS siRNA-treated hypertrophied cells (4,143.33 ± 130.47 pg/ml). C/EBPβ siRNA treatment in hypertrophied myocytes had no significant effect on secreted IL-6 (4,019.8 ± 166.67 pg/ml). Results were analyzed by one-way ANOVA followed by Tukey's post hoc test and are expressed as the mean ± SE from three independent experiments (n = 5 for each group). ***, P < 0.001 with respect to control myocytes; ††, P < 0.001 with respect to NS siRNA-treated hypertrophied myocytes. (d) Western blots showing the significant downregulation of phosphorylated STAT-3 in fibroblasts conditioned with p65 siRNA-treated hypertrophied MCM compared to fibroblasts conditioned with AngII-treated myocyte supernatant. Fibroblasts conditioned with C/EBPβ siRNA-treated hypertrophied MCM showed no
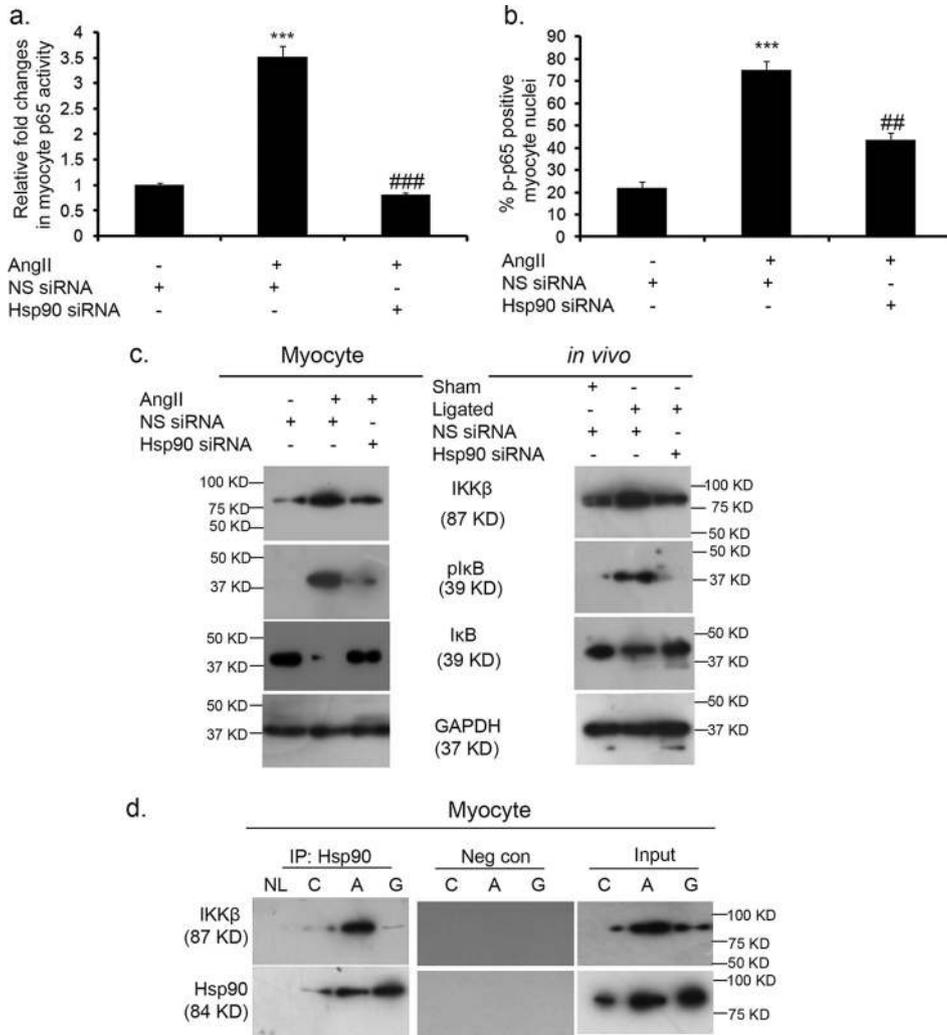
FIG 7 Hsp90 modulates IKKβ in myocytes to regulate p65 activity during hypertrophy. (a) Relative changes in luciferase assay, revealing the reduced transcriptional activity of NF-κB on the IL-6 promoter sequence in Hsp90 siRNA-treated hypertrophied myocytes compared to that in AngII-treated myocytes. Results were normalized by the *Renilla* luciferase activity in all the treatment groups ($n = 5$ for each group). ***, $P < 0.001$ with respect to control myocytes; ###, $P < 0.001$ with respect to hypertrophied myocytes. (b) Graphical representation of the results of the immunofluorescence study showing significantly reduced amounts of phospho-p65 (p-p65)-positive nuclei in Hsp90 siRNA-treated hypertrophied myocytes compared to AngII-treated cells ($n = 5$ for each group). ***, $P < 0.001$ with respect to the control; ##, $P < 0.01$ with respect to hypertrophied myocytes. (c) Western blot analysis showing the downregulated expression of IKKβ and the ratio of phosphorylated IκB (p-IκB)/total IκB upon Hsp90 inhibition in hypertrophy groups both *in vitro* and *in vivo* ($n = 10$ for each group). GAPDH was used as an internal loading control. (d) Coimmunoprecipitation experiments were done using anti-Hsp90 antibody followed by immunoblotting with an anti-IKKβ antibody *in vitro*. 17-AAG treatment significantly reduced the binding of IKKβ to Hsp90 compared to that for AngII-treated myocytes ($n = 5$ for each group). Lane NL, no lysate; lanes C, control myocytes; lanes A, AngII-treated myocytes; lanes G, 17-AAG-treated hypertrophied myocyte. The cells in lanes C and A were also treated with DMSO. IP, immunoprecipitation; Neg con, negative control.

blasts conditioned with either Hsp90 siRNA-treated hypertrophied MCM (5% ± 2%) or GW4869-treated hypertrophied MCM (3% ± 1%) (Fig. 11a).

Delayed activation of STAT-3 in fibroblasts is mediated by myocyte-secreted exosomal IL-6. Conditioning of fibroblasts with GW4869-treated hypertrophied myo-

FIG 6 Legend (Continued)

significant alteration in STAT-3 phosphorylation. GAPDH was used as an internal loading control ($n = 10$ for each group). (e) RT-PCR analyses showing significant downregulation in collagen expression in fibroblasts conditioned with p65 siRNA-treated hypertrophied MCM compared to fibroblasts conditioned with AngII-treated myocyte supernatants. Fibroblasts conditioned with C/EBPβ siRNA-treated hypertrophied MCM showed no significant alteration in collagen gene expression. *Rpl-32* was used as an internal loading control ($n = 10$ for each group).
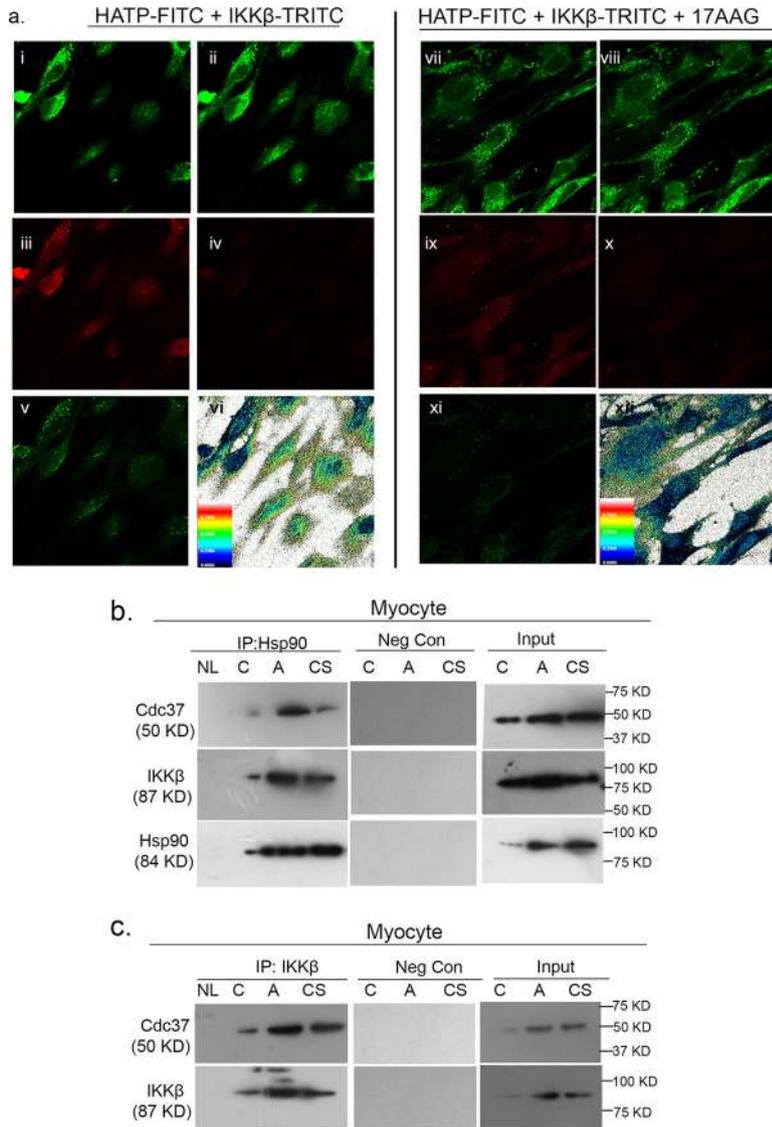
FIG 8 The interaction between Hsp90 and IKKβ is facilitated by Cdc37 during myocyte hypertrophy. (a) Hypertrophied myocytes were transfected with HATP-FLAG and then treated with AngII in either the presence or the absence of 17-AAG. Myocytes were probed for anti-FLAG and endogenous IKKβ expression. Cells were then stained with FLAG-FITC (donor) and IKKβ-TRITC (acceptor). TRITC was subjected to 50% photobleaching. Fluorescence recovery after photobleaching (FRAP) of the acceptor showed a positive FRET efficiency in AngII-treated cells (i to vi) which was significantly reduced by 17-AAG treatment (vii to xii). (i and vii) Prebleaching donor intensities; (ii and viii) postbleaching donor intensities; (iii and ix) prebleaching acceptor intensities; (iv and x) postbleaching acceptor intensities; (v and xi) delta donor (postbleaching − prebleaching) intensities; (vi and xii) FRET efficiencies alongside a color scale. FRET efficiencies were calculated and expressed as the mean ± SE from three independent experiments. (b) Coimmunoprecipitation experiments were done using an anti-Hsp90 antibody followed by immunoblotting with anti-IKKβ and anti-Cdc37 antibodies ($n = 5$ for each group). Lane NL, no lysate; lanes C, control myocytes; lanes A, AngII-treated myocytes; lanes CA, celastrol-treated hypertrophied myocytes. Lanes C and A were also treated with DMSO. (c) Coimmunoprecipitation experiments were done using an anti-IKKβ antibody followed by immunoblotting with an anti-Cdc37 antibody in myocytes. Celastrol treatment failed to alter the binding of Cdc37 to IKKβ compared to that in AngII-treated myocytes ($n = 5$ for each group). Lane NL, no lysate; lanes C, control myocytes; lanes A, AngII-treated myocytes; lanes CS, celastrol-treated hypertrophied myocytes. Lanes C and A were also treated with DMSO.

cyte supernatant resulted in a significant downregulation of phosphorylation of STAT-3 (2.21-fold ± 0.11-fold and 1.59-fold ± 0.11-fold for STAT-3Y705 and STAT-3S727, respectively) along with a significantly reduced level of collagen gene expression (1.68-fold ± 0.11-fold and 1.61-fold ± 0.05-fold for *Col-1* and *Col-3*, respectively) in such
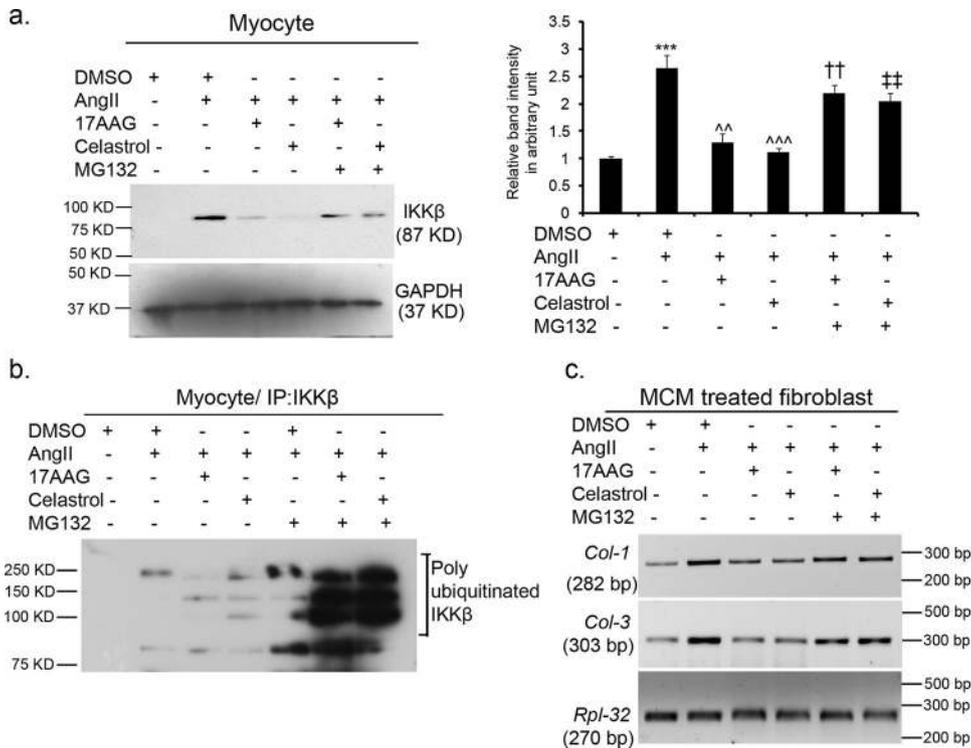
FIG 9 Formation of a ternary complex of IKKβ with Hsp90/Cdc37 in cardiomyocytes is necessary for collagen gene synthesis in fibroblasts. (a) Western blot analysis showing the restoration of IKKβ expression with simultaneous MG132 treatment in either 17-AAG-treated or celastrol-treated hypertrophied myocytes *in vitro*. GAPDH was used as an internal loading control. Results were analyzed by one-way ANOVA followed by Tukey's *post hoc* test and are expressed as the mean ± SE from three independent experiments ($n = 5$ for each group). ***, $P < 0.001$ with respect to the control; ^^^, $P < 0.001$ with respect to AngII-treated cells; ^^, $P < 0.01$ with respect to AngII-treated cells; ††, $P < 0.01$ with respect to 17-AAG-treated hypertrophied myocytes; ‡‡, $P < 0.01$ with respect to celastrol-treated hypertrophied myocytes. (b) Coimmunoprecipitation experiment showing the significantly increased polyubiquitination of IKKβ in the presence of MG132 in either 17-AAG-treated or celastrol-treated hypertrophied myocytes compared to AngII-treated cells ($n = 5$ for each group). (c) RT-PCR showing a significant restoration of *Col-1* and *Col-3* gene expression in fibroblasts treated with culture supernatants from hypertrophied myocytes subjected to simultaneous MG132 treatment in the presence of either 17-AAG or celastrol compared to that in hypertrophied MCM treated only with 17-AAG or celastrol. *Rpl-32* was used as an internal loading control ($n = 5$ for each group).

fibroblasts compared to fibroblasts conditioned with hypertrophied myocyte supernatant (Fig. 11b and c).

The effect of the myocyte supernatant on STAT-3 activation in fibroblasts was studied at different time points. Supplementation of the fibroblast culture with the AngII-treated myocyte supernatant resulted in STAT-3 phosphorylation in these cells that was maintained through the time course from 3 h until 12 h, while Hsp90 siRNA-treated hypertrophied myocyte supernatant-conditioned fibroblasts showed downregulated STAT-3 phosphorylation at similar time points. When the AngII-treated myocyte supernatant was neutralized with IL-6-neutralizing antibody, it failed to activate STAT-3 at an earlier time point (3 h), although it had a significant late-phase induction of STAT-3 phosphorylation (at 12 h) in myocyte-conditioned fibroblasts. The GW4869-treated hypertrophied myocyte supernatant did not affect the early induction of STAT-3 in myocyte-conditioned fibroblasts; however, it caused a significant downregulation in STAT-3 phosphorylation at 12 h compared with that at 3 h (Fig. 12a and b).

DISCUSSION

Increased collagen synthesis in cardiac fibroblasts as a result of prohypertrophic modules of cardiomyocytes has long been known. However, the precise mechanism of cardiac fibroblast-cardiomyocyte cross talk in the cardiac fibrosis process is still poorly
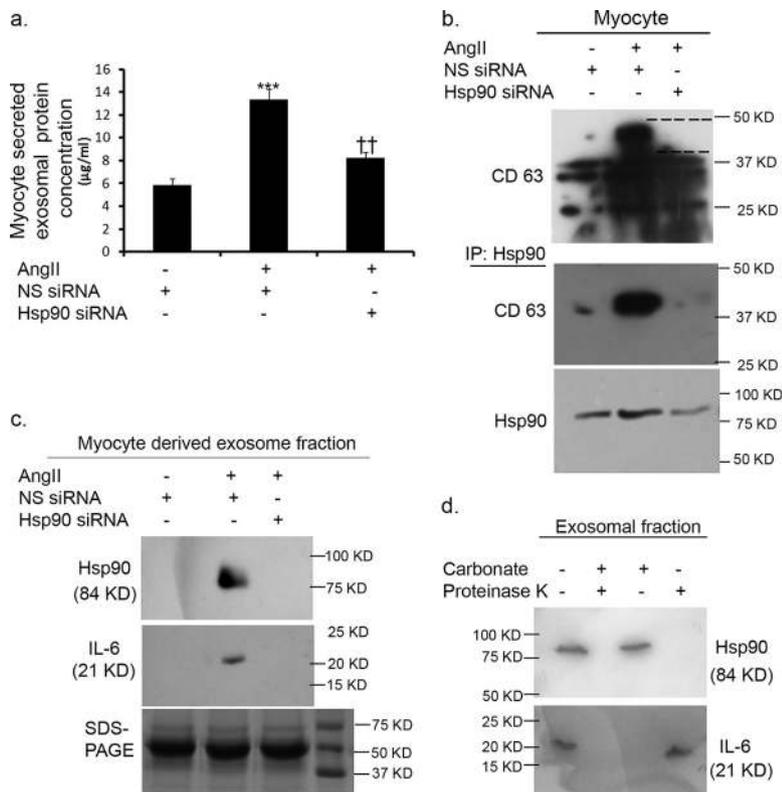
FIG 10 Hsp90 inhibition alters the release of myocyte-derived exosomes containing IL-6 during hypertrophy. (a) A micro-BCA assay showed a significant reduction in the exosomal protein content in Hsp90 siRNA-treated hypertrophied myocytes compared to that in AngII-treated myocytes. Results are expressed as the mean ± SE from three independent experiments ($n = 10$ for each group). ***, $P < 0.001$ with respect to the control; ††, $P < 0.01$ with respect to AngII-treated myocytes. (b) Immunoprecipitation with anti-Hsp90 antibody followed by Western blot analyses with CD63 and Hsp90 showing an interaction between Hsp90 and a specific glycosylated form of CD63 during myocyte hypertrophy. Western blot analysis alone showed several glycosylated forms of CD63 in the different treatment groups ($n = 10$ for each group). (c) Western blots of a myocyte-derived exosomal isolate showing the presence of Hsp90 and IL-6 only in AngII-treated myocyte-derived exosomes. A major band from a Coomassie blue-stained SDS-polyacrylamide gel of fractionated exosomal proteins was used as a loading control ($n = 5$ for each group). (d) Western blot analysis revealed the presence of Hsp90 in the exosomal membrane after carbonate treatment. Hsp90 was removed by subsequent treatment with proteinase K. IL-6 was present in exosome isolates treated only with proteinase K ($n = 3$ for each group).

understood. The present study gives us a mechanistic insight by analyzing the novel role of Hsp90 from cardiomyocytes in the regulation of collagen synthesis in cardiac fibroblasts during cardiac hypertrophy. A recent report suggested a role of fibroblast-derived microRNA-enriched exosomes as a potential regulator of cardiomyocyte hypertrophy (31). Our study also demonstrates for the first time the mechanism of Hsp90-mediated modulation of IL-6 from cardiomyocytes either in secreted forms or in exosomal forms, in which IL-6 alters the fibrotic responses in fibroblasts via biphasic STAT-3 activation during progression of the disease.

The STAT-3-dependent mechanism of collagen synthesis in fibroblasts has been well documented (9, 32). Although a direct interaction between STAT-3 and Hsp90 has been reported previously (21–23), our previous findings suggested that Hsp90 inhibition in cardiac fibroblasts alone had no effect on STAT-3 activation *in vitro* (Fig. 1a). Hsp90 inhibition also failed to exert any effect on STAT-3 signaling in isolated hypertrophied myocytes (Fig. 1b). However, Hsp90 inhibition in rats in which the renal artery was ligated together with myocyte-specific Hsp90 knockdown *in vivo* led to deactivation of the STAT-3 signal along with the regression of fibrosis and a consequent improvement in cardiac function during cardiac hypertrophy (Fig. 2a and 3a and c to e). This observation led us to believe that the *in vitro* and *in vivo* effects of Hsp90 inhibition are
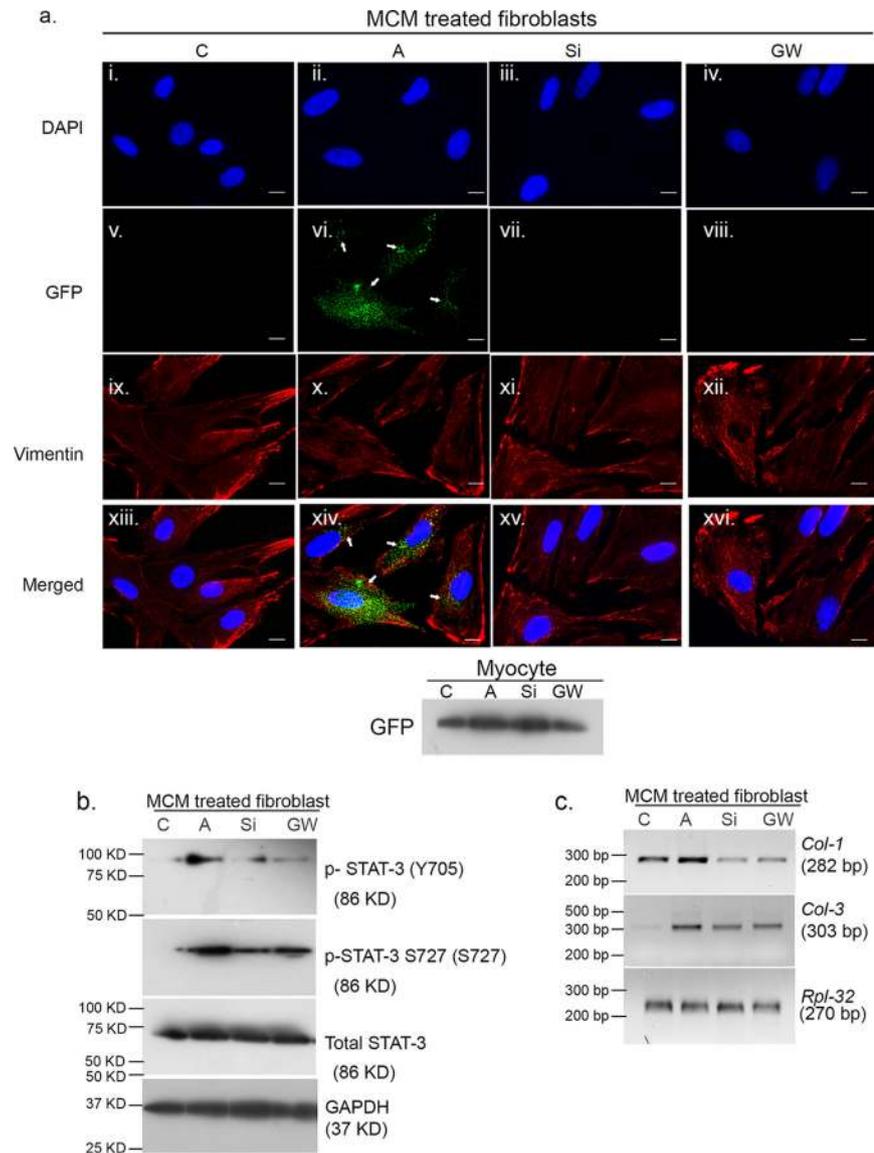
FIG 11 The transmigration of myocyte-derived exosomes is critical in the regulation of STAT-3-mediated collagen gene expression in fibroblasts during hypertrophy. (a) Immunofluorescence study showing the presence of myocyte-derived exosomes (green fluorescence) in fibroblasts conditioned with CD63-eGFP-transfected hypertrophied myocyte supernatants. Either Hsp90 siRNA or GW4869 treatment of CD63-eGFP-transfected hypertrophied myocytes inhibited the transmigration of myocyte-derived exosomes into the MCM-treated fibroblasts. Fibroblasts were stained with primary antibody against vimentin (red fluorescence), and nuclei were stained with DAPI ($n = 5$ for each group). (i to iv) DAPI staining; (v to viii) GFP-positive cells (marked by arrows); (ix to xii) vimentin expression; (xiii to xvi) merged images. Immunoblotting of myocytes with an anti-GFP antibody confirmed the equal transfection of CD63. C, fibroblasts conditioned with control MCM; A, fibroblasts treated with hypertrophied MCM; Si, fibroblasts conditioned with Hsp90 siRNA-treated hypertrophied MCM; GW, fibroblasts conditioned with GW4869-treated hypertrophied MCM. Control and hypertrophied myocytes were treated with either DMSO or NS siRNA, yielding similar results. Bars, 20 μm. Magnification, ×100. (b) Western blot analysis revealed the significant downregulation of phosphorylated STAT-3 in fibroblasts conditioned with the GW4869-treated hypertrophied myocyte supernatant compared to fibroblasts conditioned with the AngII-treated myocyte supernatant. GAPDH was used as an internal loading control ($n = 5$ for each group). Lanes C, fibroblasts conditioned with control MCM; lanes A, fibroblasts treated with hypertrophied MCM; lanes Si, fibroblasts conditioned with Hsp90 siRNA-treated hypertrophied MCM; lanes GW, fibroblasts conditioned with GW4869-treated hypertrophied MCM. Control and hypertrophied myocytes were treated with either DMSO or NS siRNA, yielding similar results. (c) RT-PCR showing significantly reduced levels of collagen gene expression in fibroblasts conditioned with GW4869-treated hypertrophied MCM compared to that in fibroblasts conditioned with the AngII-treated myocyte supernatants. *Rpl-32* was used as an internal loading control ($n = 5$ for each group). Lanes C, fibroblasts conditioned with control MCM; lanes A, fibroblasts treated with hypertrophied MCM; lanes Si, fibroblasts conditioned with Hsp90 siRNA-treated hypertrophied MCM; lanes GW, fibroblasts conditioned with GW4869-treated hypertrophied MCM. Control and hypertrophied myocytes were treated with either DMSO or NS siRNA, yielding similar results.
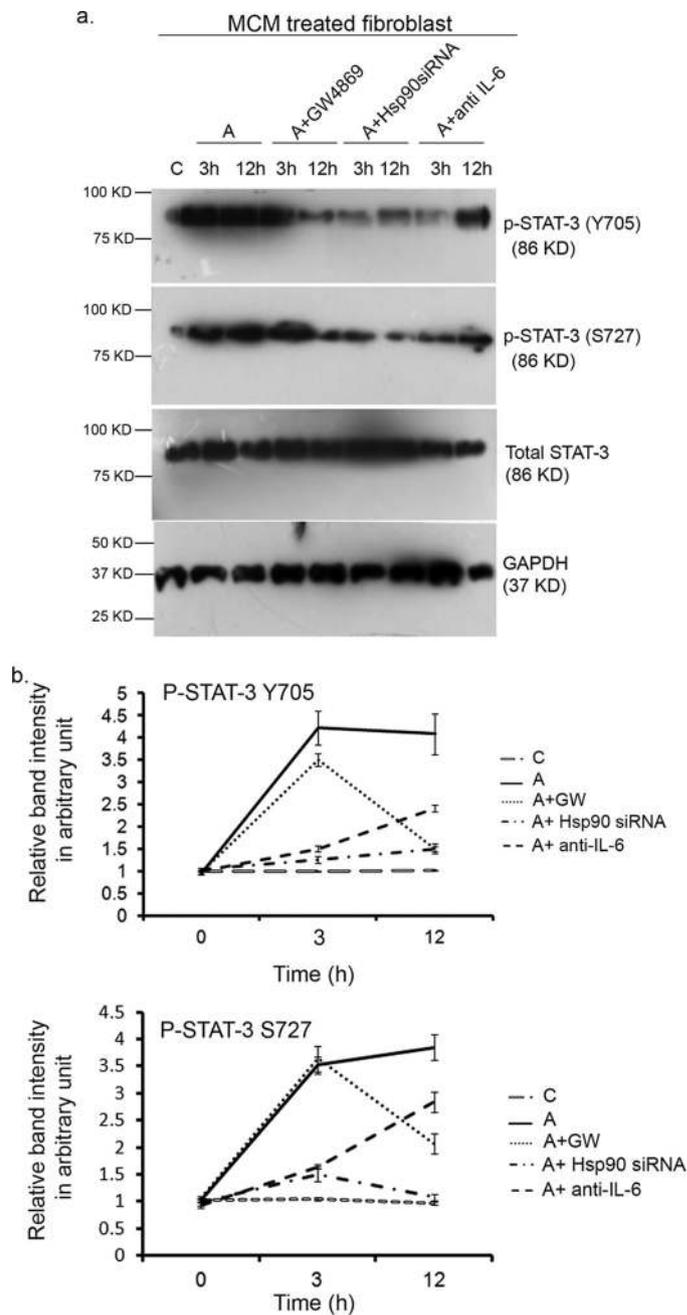
FIG 12 Hsp90 of myocytes is critical in the temporal regulation of STAT-3 activation in fibroblasts during cardiac hypertrophy. (a) Western blot analysis showing changes in the ratio of phosphorylated STAT-3/total STAT-3 at different time points in fibroblasts conditioned with culture supernatants of myocytes subjected to various treatments ($n = 5$ for each group). GAPDH was used as an internal loading control. (b) Graphical representations of the Western blots shown in panel a showing temporal changes in STAT-3 phosphorylation. Results were analyzed by one-way ANOVA followed by Tukey's *post hoc* test. C, fibroblasts conditioned with control MCM; A, fibroblasts conditioned with hypertrophied MCM; A+GW, fibroblasts conditioned with GW4869-treated hypertrophied MCM; A+Hsp90 siRNA, fibroblasts conditioned with Hsp90 siRNA-treated hypertrophied MCM; A+anti-IL-6, fibroblasts conditioned with anti-IL-6 neutralizing antibody-treated hypertrophied MCM. Control and hypertrophied myocytes were treated with either DMSO, NS siRNA, or NS IgG, yielding similar results.

different and Hsp90 inhibition in myocytes might have an indirect effect on collagen synthesis in cardiac fibroblasts. To have an insight into the underlying cellular influence of myocytes, fibroblasts were conditioned with Hsp90-inhibited hypertrophied myocytes or their culture supernatant, which produced a significant downregulation of

STAT-3 activity as well as subsequently reduced the level of collagen gene expression in myocyte-conditioned fibroblasts. This clearly indicates that paracrine factors from myocytes can regulate STAT-3 activation in fibroblasts (Fig. 2c and 3a and b).

The autocrine/paracrine effect of IL-6 type cytokines upon STAT-3 activation is a well-known phenomenon found to occur in several cell types (9, 13–15). Fredj et al. (33) reported a paracrine role of myocyte-secreted IL-6 in fibroblast proliferation. In our study, Hsp90 inhibition, which led to decreased levels of IL-6 production in hypertrophied cardiomyocytes together with decreased levels of STAT-3 activation in myocyte-conditioned fibroblasts, pointed to a probable role of Hsp90 of the myocytes in IL-6-mediated paracrine regulation of STAT-3 in fibroblasts (Fig. 4). This was further confirmed by conditioning fibroblasts with an IL-6-neutralized hypertrophied myocyte supernatant, which resulted in reduced levels of STAT-3 phosphorylation and the subsequent downregulation of collagen synthesis compared to the findings for fibroblasts conditioned with AngII-treated myocyte supernatant (Fig. 5). An IL-6 activity assay indicated significantly higher levels of activity of IL-6 secreted from hypertrophied myocytes than IL-6 secreted from AngII-treated fibroblasts (Fig. 4a), suggesting that myocyte-derived IL-6 plays a pivotal paracrine role in the regulation of STAT-3-mediated fibrotic signaling, while the autocrine action of IL-6 on cardiac fibroblasts is merely significant during AngII-mediated cardiac hypertrophy. In addition to IL-6, IL-11 and LIF were reported in human adult ventricular myocyte culture supernatants (34). However, it was observed that the levels of IL-11 and LIF secreted from hypertrophied cardiomyocytes were significantly less than the levels of IL-6 secreted under similar conditions, and moreover, the levels of IL-11 and LIF remained unaltered by Hsp90 siRNA treatment (data not shown). Myocyte-derived IL-6 thus surfaced as a major player in the regulation of STAT-3-mediated collagen expression in fibroblasts during cardiac hypertrophy.

As reported earlier, IL-6 promoters contain a putative p65 binding site, and thus, the synthesis of IL-6 is tightly regulated by p65 in different cell types (35, 36). Apart from p65, earlier reports also provided evidence of the positive regulation of the IL-6 gene by the C/EBP and AP-1 families of proteins (37, 38). Our study has shown that Hsp90 inhibition in hypertrophied myocytes significantly downregulated the nuclear expression of both p65 and C/EBPβ (Fig. 6a and b); however, no change in the levels of AP-1 expression (c-*fos* and c-*jun*) were observed under similar treatment conditions (data not shown). To further assess the roles of p65 and C/EBPβ in IL-6 expression during hypertrophy, hypertrophied myocytes were treated with either p65 siRNA or C/EBPβ siRNA. Although p65 knockdown in hypertrophied myocytes resulted in the significant downregulation of secreted IL-6, C/EBPβ knockdown failed to alter IL-6 secretion from these cells, indicating that altered IL-6 expression during cardiac hypertrophy is predominantly regulated by p65 and not by C/EBPβ (Fig. 6c), as was previously reported during hypoxia (39). Reduced levels of C/EBPβ expression by Hsp90 inhibition could be attributed to the reduced IL-6 levels found under similar conditions in hypertrophied myocytes, as reported previously by Stephanou et al. (40), who showed a probable role of IL-6 in the regulation of C/EBPβ expression.

In an effort to decipher the role of p65 and C/EBPβ in the regulation of STAT-3-mediated collagen synthesis, it was observed that p65 knockdown in hypertrophied myocytes significantly downregulated STAT-3 phosphorylation as well as the levels of collagen gene expression, whereas C/EBPβ knockdown failed to alter the expression of either of these proteins in hypertrophied MCM-treated fibroblasts (Fig. 6d and e), thereby establishing the pivotal role of myocyte-derived p65 in the regulation of collagen expression in fibroblasts during hypertrophy.

Induction of p65 during cardiac hypertrophy has previously been associated with the fate of cardiomyocytes (41); however, the significance of p65 upregulation in hypertrophied cardiomyocytes has not yet been colligated to excess collagen synthesis in fibroblasts. Our data revealed decreased levels of nuclear translocation of p65 in Hsp90-inhibited hypertrophied myocytes and, subsequently, a reduced level of tran-

scriptional activity of p65 in these cells, suggesting that Hsp90 modulates IL-6 synthesis in myocytes via alteration of its p65 activity (Fig. 7a and b).

Classically, p65 activation requires phosphorylation of IKKβ, which in turn phosphorylates IκB to relieve its inhibition of p65, and the free p65 then translocates to the nucleus to bind to the promoters of its target genes (42). The requirement for Hsp90 in such activation of IKKβ and its downstream signaling cascade has been described previously (43, 44). Lee et al. (45) already reported on the role of Hsp90 in IKKβ-mediated p65 activation during myocyte hypertrophy *in vitro*. Myocyte-targeted knockdown of Hsp90 in our study, which led to the reduced activation of the IKKβ-p65 axis during cardiac hypertrophy, corroborated the earlier reports (Fig. 7c). Coimmunoprecipitation of IKKβ with Hsp90 during cardiac hypertrophy *in vitro* and *in vivo* provided evidence of physical interactions between these proteins, and the inability of IKKβ to immunoprecipitate with Hsp90 in the presence of 17-AAG confirmed the specificity of such interactions (Fig. 7d). FRET-FRAP analysis showed significant FRET efficiency, indicating that direct physical interactions exist between IKKβ and the ATPase domain of Hsp90 (Fig. 8a). The significantly reduced FRET efficiency during 17-AAG treatment again confirmed the specificity of such interactions.

Cdc37 had been shown to interact with Hsp90 during the processing of its client kinases (46, 47). Our results clearly showed that disruption of the Hsp90-Cdc37 interaction by celastrol treatment during hypertrophy abrogated subsequent interactions between Hsp90 and IKKβ in myocytes, indicating that the Hsp90-Cdc37 interaction is essential to stabilize IKKβ prior to the formation of a ternary complex with Hsp90. However, the blockage of Hsp90-Cdc37 interactions did not alter the binding of Cdc37 and IKKβ, thus indicating that Cdc37 might ensure the efficient loading of IKKβ on Hsp90, resulting in the activation of p65 and subsequent IL-6 synthesis in hypertrophied myocytes. The downregulated expression of IKKβ, consistent with the loss of its interaction with Hsp90, raises questions about the fate of IKKβ in Hsp90-inhibited hypertrophy samples (Fig. 8b and c).

The ubiquitination of IKKβ during Hsp90 inhibition was previously reported (44). Our data showed the restoration of IKKβ expression and increased polyubiquitination either in 17-AAG-treated or in celastrol-treated hypertrophied myocytes in the presence of a proteasome inhibitor, MG132 (Fig. 9a and b). This suggests that ubiquitin-mediated proteasomal degradation plays a key role in the downregulation of IKKβ in the absence of active chaperoning by the Hsp90/Cdc37 complex during AngII-mediated myocyte hypertrophy. These results altogether indicate that the stabilization of functional IKKβ depends on its physical interaction with Hsp90 and that the loss of such interactions during 17-AAG or celastrol treatment renders IKKβ vulnerable to ubiquitin-mediated proteasomal degradation and results in the subsequent loss of p65-induced transcription of IL-6 in hypertrophied myocytes. Fibroblasts conditioned with supernatants of MG132-treated hypertrophied myocytes along with 17-AAG or celastrol showed a significant restoration of regressed collagen expression compared with that in fibroblasts conditioned with similar myocyte supernatants without proteasomal inhibition (Fig. 9c). This indicates that the modulation of IKKβ by Hsp90 in the myocyte is necessary for collagen gene expression in fibroblasts during cardiac hypertrophy.

Besides occurring in a secreted form, IL-6 may also reside in cell-derived exosomes, as suggested earlier (48). Myocyte-derived exosomes have not yet been characterized during AngII-mediated hypertrophy. Our study showed a significant increase in the myocyte-derived exosome content during hypertrophy, which was again reduced by knocking down Hsp90 expression in myocytes (Fig. 10a).

One pertinent question was how Hsp90 regulates exosomal release from myocytes. However, the regulation of exosome release has not been well documented in any system so far. Glycosylation of CD63 was reported in various cell types, and CD63 knockdown resulted in decreased exosomal release (49–51). This prompted us to check the expression of CD63 in treated myocytes, which revealed a significantly altered pattern of glycosylation of CD63 by Hsp90 knockdown in hypertrophied cells, along with a decrease in the amount of exosome released compared to the amount released

from AngII-treated cells (Fig. 10a and b). Such an altered glycosylation of CD63 in the absence of Hsp90 might play a role in the modulation of myocyte-derived exosomal release during cardiac hypertrophy. However, the relation between Hsp90 and CD63 was poorly understood. A coimmunoprecipitation experiment revealed a positive interaction of Hsp90 with a specific pattern of glycosylation of CD63 in hypertrophied myocytes that was significantly downregulated by Hsp90 siRNA treatment (Fig. 10b). Taken together, our results thus indicate that the interaction between Hsp90 and glycosylated CD63 might be a crucial regulator of exosome release from myocytes during hypertrophy. However, further studies in this direction might elucidate the precise mechanism of Hsp90 in the modulation of exosomal release during cardiac hypertrophy.

Exosomes derived from hypertrophied myocytes were further characterized. Hsp90 and IL-6 were found to be incorporated into exosomes derived from hypertrophied myocytes (Fig. 10c). The presence of Hsp90 in exosomes has been reported previously (52); however, the precise location of Hsp90 in myocyte-derived exosomes was unknown. Treatment of exosomes with carbonate and proteinase K revealed the presence of IL-6 inside the lumen and showed that Hsp90 was an adherent protein on the surface of the exosomal membrane (Fig. 10d), as observed by Gupta and Knowlton (53) in the case of Hsp60. Identifying their precise location within myocyte-derived exosomes might provide important clues to decipher the mechanism of exosome-mediated signaling pathways in fibroblasts during cardiac hypertrophy and fibrosis.

Extracellular Hsp90-mediated modulation of proinflammatory cytokines has been reported earlier (54). The autocrine effect of TNFR-1 in myocyte-derived exosomes during hypoxia and the paracrine effect on myocytes by IL-6-containing exosomes from macrophages during sepsis were shown previously (55, 56). However, it was still unclear whether the same myocyte-derived exosomes can transmigrate to fibroblasts, thereby initiating fibrosis. Colocalization experiments showed a significant amount of GFP-positive fibroblasts when fibroblasts were conditioned with supernatants derived from hypertrophied myocytes transfected with CD63-enhanced green fluorescent protein (eGFP). This indicated the transmigration of myocyte-derived exosomes with its content to fibroblasts during cardiac hypertrophy (Fig. 11a, panels vi and xiv). When exosome release was blocked in hypertrophied myocytes, GW4869-treated myocyte supernatant-conditioned fibroblasts showed a significant reduction in STAT-3 activity and subsequent collagen synthesis (Fig. 11b and c). Interestingly, Hsp90 inhibition also led to reduced exosome release during myocyte hypertrophy, indicating a potential role of Hsp90 in the regulation of exosome-mediated STAT-3 activation in fibroblasts.

To have a better insight into the effect of myocyte-derived exosomes on STAT-3 signaling in fibroblasts, time-dependent STAT-3 phosphorylation was assessed. The delayed activation of STAT-3 in vascular smooth muscle cells and in response to tumor-derived exosomes in THP-1 cells has been reported (48, 57). In this study, exosomal blockade in hypertrophied cardiomyocytes had no effect on STAT-3 phosphorylation in myocyte-conditioned fibroblasts at earlier time points; however, it dampened STAT-3 activity at later phases. IL-6 neutralized the hypertrophied myocyte supernatant; on the other hand, it abolished STAT-3 phosphorylation at earlier time points but failed to do so in the later phases. These results indicate that the effect of secreted IL-6 and exosomal IL-6 on STAT-3 activation in fibroblasts was temporally different. While IL-6 secreted from myocytes is presumed to be required for the early induction of STAT-3 phosphorylation, exosomal IL-6 might have a delayed role in the maintenance of STAT-3 activation in fibroblasts. Also, knockdown of Hsp90 in hypertrophied myocytes abrogated STAT-3 phosphorylation throughout the time course, confirming its role in the regulation of biphasic activation of STAT-3 in fibroblasts (Fig. 12a and b).

Our study proposes a novel signaling mechanism where Hsp90 orchestrates the synthesis of IL-6 and its release in exosomes from myocytes during cardiac hypertrophy. IL-6 secreted from such myocytes and IL-6 secreted from myocyte-derived exosomes are together responsible for the activation and maintenance of STAT-3 signaling in
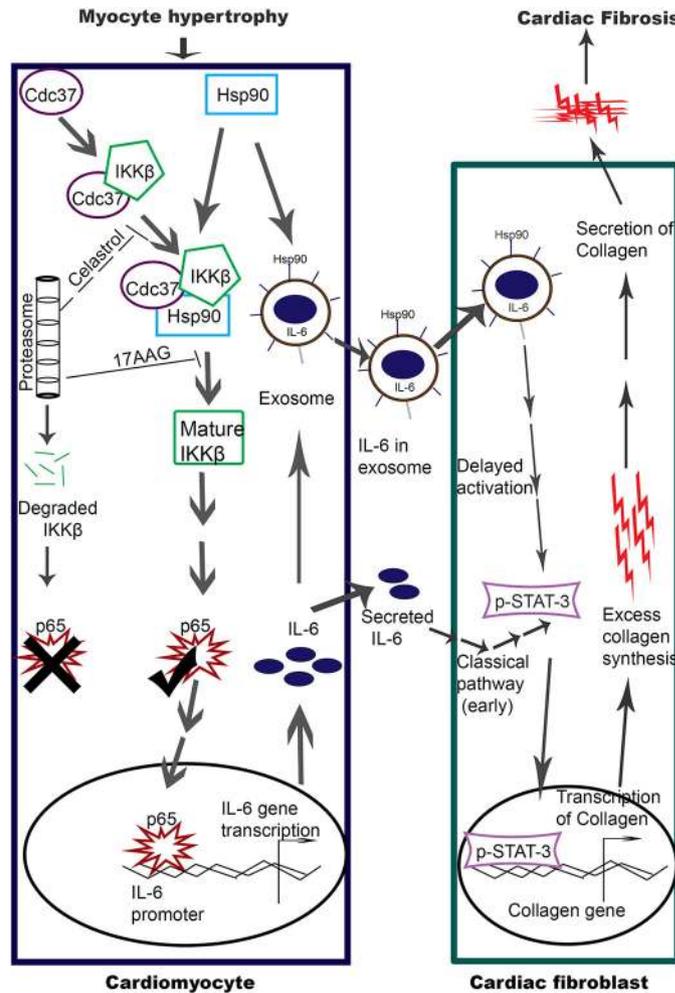
FIG 13 Schematic representation of a plausible pathway for Hsp90-mediated regulation of STAT-3 that subsequently alters collagen gene expression during cardiac hypertrophy involving myocyte-fibroblast cross talk.

cardiac fibroblasts, resulting in excess collagen synthesis and deposition in the diseased myocardium during cardiac hypertrophy (Fig. 13). In conclusion, our data reveal for the first time a profibrotic role exerted by Hsp90 of the myocytes via the regulation of myocyte-synthesized IL-6 and the biphasic activation of STAT-3 in fibroblasts. Future studies are required to resolve the mechanism of IL-6 incorporation into the exosomes and its release in the *in vivo* system to develop a better therapeutic regime to treat cardiac hypertrophy and fibrosis.

MATERIALS AND METHODS

Animals used. The 28-week-old male Wistar rats used in this study ($n = 40$) were procured from the National Institute of Nutrition, Hyderabad, AP, India. The investigation conforms with the guidelines in the *Institutional Administrator's Manual for Laboratory Animal Care and Use*, published by the National Institutes of Health (58), and was also approved by the Institutional Animal Ethics Committee, University of Calcutta (registration number 885/ac/05/CPCSEA), and registered with the Committee for the Purpose of Control and Supervision of Experiments on Laboratory Animals (CPCSEA), Ministry of Environment and Forests, Government of India.

Cell culture techniques. Neonatal cardiomyocytes and fibroblasts were cultured and treated as described in the following sections. For coculture experiments, culture supernatants from different experimental groups of myocytes were transferred to fibroblast plates and were conditioned for 24 h (myocyte-conditioned medium [MCM]-treated fibroblasts). Also, fibroblasts were cocultured with myocytes on coverslips and inserts (7). For time point analysis, fibroblasts were incubated with MCM for 3 h to 12 h.

(i) Culture of neonatal cardiomyocytes. Neonatal myocytes were isolated from the hearts of 2- to 3-day-old rat pups and cultured on laminin-coated standard six-well plates (Sigma-Aldrich, St. Louis, MO) using a previously described procedure (59), and cover glasses were placed on the plates. On the third day, myocytes were incubated in serum-starved Dulbecco modified Eagle medium for 8 to 12 h before experimentation. Approximately 90% pure isolated cardiomyocytes were confirmed by staining with α-actinin antibody (41).

(ii) Treatment of neonatal cardiomyocytes. Neonatal rat cardiomyocytes were incubated for 24 h at 37°C in the absence (control) or presence (treated) of 10^{-8} mol/liter Sar1 AngII (Bachem, Torrance, CA). AngII was replenished every 6 h throughout the incubation period (41). Myocytes were treated with 1 μM the Hsp90 inhibitor 17-allylamino-17-demethoxygeldanamycin (17-AAG; Sigma), 2 μM the Hsp90-Cdc37 interaction blocker celastrol (Sigma-Aldrich, St. Louis, MO), 20 μM the proteasome inhibitor MG132 (Z-Leu-Leu-Leu-Ala; Sigma-Aldrich, St. Louis, MO), and 20 μM the exosome release blocker GW4869 (Sigma-Aldrich, St. Louis, MO) for 2 h prior to AngII treatment as previously described (26). An equivalent concentration of dimethyl sulfoxide (DMSO) was added for the other experimental groups where applicable. In the case of GW4869 treatment, cell culture supernatants were collected after the treatment period for the determination of AchE activity in order to confirm successful exosome release blockade. Myocytes were also treated with neutralizing antibodies to IL-6 (Abcam, UK). Cells in the other treatment groups were treated with an equivalent amount of a goat IgG isotype control (Thermo Fisher, MA). Treatment of myocytes with anti-p65 RelA siRNA, anti-C/EBPβ siRNA, Hsp90 ab1 siRNA (Qiagen Flexitube siRNA), or negative-control siRNA (catalogue no. 1027280; AllStars negative-control siRNA; Qiagen) was done using the HiPerfect transfection reagent (Qiagen) per the manufacturer's instruction.

(iii) Isolation and treatment of cardiac fibroblasts. Cardiac fibroblasts were isolated from the hearts of 28-week-old rats by the collagenase dispersion method described by Mir et al. (9). Cells were maintained at 37°C with 5% CO_2 and were subsequently passaged. Fibroblasts were confirmed by staining with antivimentin antibody. The treatment of fibroblasts with AngII, 17-AAG, and Hsp90 siRNA was done as previously described (26).

Generation of cardiac hypertrophy *in vivo*. Cardiac hypertrophy *in vivo* was generated by ligating the right renal artery of 28-week-old male rats (weight, 250 to 300 g) as described earlier (9). Rats were anesthetized with an intraperitoneal (i.p.) injection of a mixture of ketamine (80 mg/kg of body weight) and xylazine (12 mg/kg). Rats that underwent a similar procedure without aortic ligation (a sham operation) were designated the control group. Animals were maintained under optimum conditions for 14 days and were sacrificed on the 15th day after surgery. Hearts were taken out and stored in liquid nitrogen for future use. Hypertrophy was measured from the heart weight (HW; in milligrams)-to-body weight (BW; in grams) ratio (41).

Administration of 17-AAG *in vivo*. 17-AAG was administered i.p. for 3 consecutive days at a dose of 0.2 mg/kg/day before renal artery ligation. Control and ligated rats were treated with equivalent amounts of DMSO (26).

Cardiomyocyte-targeted delivery of Hsp90 siRNA *in vivo*. Hsp90 siRNA was encapsulated in stearic acid-modified carboxy methyl chitosan (CMC) conjugated to a cardiomyocyte-targeting peptide at a weight ratio of 1:100 by incubation for 2 h at 4°C as described previously (60). Hsp90 siRNA with CMC-peptide was injected intravenously at a dose of 2 mg/kg of body weight into rats in which the renal artery was ligated on alternate days starting from the 8th day until the 14th day of ligation. Rats that underwent a sham operation and treated with nonspecific (NS) siRNA tagged with CMC-peptide were used as negative controls.

RT-PCR. Total RNA was isolated from cells (obtained after 24 h of treatment) and tissues (obtained on the 15th day after surgery) using the TRIzol reagent (Invitrogen) by following the manufacturer's instructions. One microgram of total RNA was used to make cDNA using a cloned avian myeloblastosis virus (AMV) first-strand cDNA synthesis kit (Invitrogen). Reverse transcription-PCR (RT-PCR) for *Col-1*, *Col-3*, and *Rpl-32* was done with appropriate primers (26).

Estimation of total collagen content by hydroxyproline assay. The total collagen content in ventricular tissue in which the renal artery was ligated as well as in the fibroblast culture supernatant was measured by a hydroxyproline assay. With the help of a standard curve, the hydroxyproline content in the unknown samples was calculated. The amount of collagen was calculated by multiplying the hydroxyproline content by a factor of 8.2 (9).

Histological analysis. Heart tissues from each group of animals were taken for analysis of the collagen volume fraction (CVF). Coronal sections obtained from the equator of the left ventricle were fixed, and sections were stained with Masson's trichrome (Sigma-Aldrich, MO) to analyze collagen deposition under a microscope (Nikon NIS BR). Thirty sections were scanned, and at least 10 images were captured from each section. Images were digitized and processed by the use of ImageJ, a computer morphometric program. CVF was calculated as the sum of all collagen-stained tissue areas of the coronal sections divided by the total surface area of the section. Color segmentation was applied to separate the stained tissues from other nonspecific objects (60).

Determination of cardiac function. Two-dimensional echocardiography was performed to determine cardiac function *in vivo*. Lightly sedated rats were evaluated using the M-mode views on a transthoracic study, measuring the left ventricular diastolic dimension (LVDD) and fractional shortening (FS; in percent). Data were correlated with the timing of the QRS complex. Digitized images were obtained using an ultrasound system (Vivid S5 system; GE Healthcare, Milwaukee, WI) (41, 61).

Protein isolation. Proteins were isolated from myocytes and adult fibroblasts using a mammalian protein extraction reagent (M-PER; Thermo Scientific, IL) according to the manufacturer's protocol.

Protein extracts were prepared from ventricular tissue using a previously described procedure (7). Nuclear fractions from tissue samples were isolated by standard differential centrifugation methods (41).

Western blotting. Western blot analysis was performed as described by Mir et al. (9). Briefly, the proteins in 30- to 50-μg protein samples were separated by 10 to 12.5% SDS-PAGE and transferred to a polyvinylidene difluoride membrane. After the membranes were blocked, they were incubated with polyclonal antibodies to Hsp90 (Abcam, UK), ubiquitin (Abcam, UK), and CD63 and C/EBPβ (Santa Cruz Biotechnology, Santa Cruz, CA), a monoclonal antibody to Cdc37 (Cell Signaling, MA), phosphorylated and total antibodies to p65, IκB, IKKβ, and STAT-3 (Cell Signaling, MA), and horseradish peroxidase (HRP)-conjugated secondary antibodies (Thermo Fisher, MA). Immunoreactive bands were visualized using an Immobilon Western chemiluminescence HRP-conjugated substrate (Millipore, MA). Glyceraldehyde-3-phosphate dehydrogenase (GAPDH) and histone deacetylase 1 (HDAC-1) (Cell Signaling, MA) were used as loading controls for cytosolic and nuclear proteins, respectively. Blots were normalized by the appropriate loading controls and were scanned and quantitated using a GelDoc XR system and Quantity One software, version 4.6.3 (Bio-Rad, CA).

Estimation of IL-6, IL-11, and LIF in culture supernatants. The amounts of IL-6, LIF, and IL-11 secreted in the culture supernatants of the different groups were estimated by the use of respective ELISA kits (an IL-6 ELISA kit [RayBiotech] and IL-11 and LIF ELISA kits [MyBioSource]) following the manufacturers' protocols. Results are expressed as the number of picograms of cytokine per milliliter of culture supernatant.

Immunofluorescence study. Myocytes grown on coverslips were treated with AngII and Hsp90 siRNA as described above and then stained with the primary antibodies for actinin and phospho-p65 (Cell Signaling, MA), followed by incubation with Alexa Fluor 488- and Alexa Fluor 633-labeled secondary antibodies (Molecular Probes) as previously described (9). After the slides were mounted with Vectashield (with DAPI [4′,6-diamidino-2-phenylindole]) (Vector Laboratories, CA), the slides were examined under a confocal microscope (FV1200; Olympus, Singapore).

An immunofluorescence study was performed *in vivo* with frozen ventricular tissue sections (4 mm), prepared using a CM1850 cryostat (Leica, CA), from the different experimental groups. The tissue sections were fixed and stained with antibodies against IL-6 (Santa Cruz Biotechnology, Santa Cruz, CA) and sarcomeric alpha-actinin (Abcam, UK), followed by incubation with labeled secondary antibodies and mounting with DAPI.

Coimmunoprecipitation. Coimmunoprecipitation was done following the manufacturer's protocol (Pierce coimmunoprecipitation kit; Thermo Fisher, MA). Briefly, proteins were incubated with fast-flow protein G- or protein A-Sepharose beads and centrifuged to eliminate nonspecifically bound proteins (62). The concentration of the precleared proteins was estimated by Bradford's assay. Two hundred micrograms of protein was immunoprecipitated using the primary antibodies anti-IKKβ and anti-Hsp90, respectively. The immunoprotein complex was again incubated with protein G- or protein A-Sepharose beads. Attached proteins were then eluted from the beads in 1% SDS buffer, followed by immunoblotting with monoclonal antibodies against Cdc37 and ubiquitin (26). Normalization was done by immunoblotting using the same antibodies.

Measurement of transcriptional activity of NF-κB by Dual-Luciferase assay. IL-6–luciferase and pRL-TK were used for the Dual-Luciferase NF-κB reporter assay (Promega), performed according to the manufacturer's protocol. Briefly, myocytes were plated on six-well plates and transfected with 3 μg of reporter plasmid carrying the firefly luciferase gene under the control of the IL-6 promoter containing the NF-κB binding consensus sequence (PGL-3) and 3 μg of reference plasmid pRL-TK carrying the *Renilla* luciferase gene under the control of the simian virus 40 enhancer and promoter (Promega). The Lipofectamine 2000 reagent (Invitrogen) was used as a transfection reagent following the manufacturer's protocol. After 16 h, cells were treated with 17-AAG followed by AngII and kept for another 24 h. Cells were lysed in 200 μl of passive lysis buffer (Promega). Firefly luciferase and *Renilla* luciferase activities in 20 μl of cell lysate were measured by use of a Dual-Luciferase reporter assay system (Promega) and a luminometer (Varioskan multimode reader; Thermo Fisher, MA). Relative activity was defined as the ratio of firefly luciferase activity to *Renilla* luciferase activity.

Plasmid construction and transfection. The Hsp90 ATPase domain (HATP; nucleotides 148 to 610, corresponding to amino acids 36 to 190 of Hsp90 ab1) was amplified from extracted RNA by RT-PCR and cloned in frame into the FLAG vector (HATP-FLAG) as previously described (26). The plasmid expressing CD63-eGFP was a kind gift from Paul Luzio's lab (Addgene). All the clones were confirmed by sequencing (3730 DNA analyzer; Applied Biosystems). Plasmids were transfected to AngII-treated cardiomyocytes with the help of the TurboFect transfection reagent (Thermo Scientific, IL) per the manufacturer's protocol.

FRAP. Hypertrophied myocytes were transfected with HATP-FLAG in either the presence or the absence of 17-AAG. Cells were then stained with FLAG-fluorescein isothiocyanate (FITC) and IKKβ-tetramethyl rhodamine isocyanate (TRITC). The FITC and TRITC dyes were used as the donor and acceptor, respectively, in this fluorescence recovery after photobleaching (FRAP) analysis. TRITC was subjected to 50% photobleaching, and the intensity of FITC was measured. Fluorescence resonance energy transfer (FRET) efficiency was calculated from the difference between the postbleaching and prebleaching donor intensities (delta donor) using a confocal microscope (FV1200; Olympus) (26).

Isolation of exosome from myocyte-conditioned medium. Exosomes were isolated according to the method of Savina et al. (63, 64). Briefly, 5 ml of medium was collected on ice and centrifuged first at 800 × g for 10 min to remove any cells and then at 12,000 × g for 30 min to eliminate any cellular debris. Exosomes were then separated from the supernatant by centrifugation at 110,000 × g for 2 h. The

exosomal pellet was washed once in phosphate-buffered saline (PBS) and then resuspended in 200 μl of PBS (exosomal fraction) (53, 65).

Characterization of exosomal proteins. (i) Determination of the quantity of exosomes. The quantity of exosomes was determined by a micro-BCA assay (Pierce, Rockford, IL) by measuring the total amount of exosomal protein (55).

(ii) Carbonate treatment. Exosomes were treated with 1 M Na_2CO_3, pH 11.5, for 30 min at 37°C. Carbonate treatment opens and flattens membranes, releasing proteins that are not integrated into the membrane (53).

(iii) Proteinase K treatment. Carbonate-treated exosomes were resuspended in either 7 mM proteinase K, 10 mM EDTA, 5 mM *N*-ethylmaleimide (NEM) or 10 nM EDTA, 5 mM NEM as a control. The membranes were incubated at 37°C for 10 min, which digests proteins that are present on the surface of the membrane. The membranes were then centrifuged and resuspended in sample buffer (53).

Identification of myocyte-derived exosomes in fibroblasts. The plasmid expressing CD63-eGFP was transfected into myocytes followed by different treatments. Cell culture supernatants from all the treatment groups were transferred to the respective fibroblast plates, and the plates were incubated for 24 h. Fibroblasts were then stained with antivimentin antibody (Abcam, UK), and the presence of GFP was observed after mounting with DAPI under a fluorescence microscope (Nikon NIS BR). Equal transfection of CD63-eGFP in myocytes was confirmed by immunoblotting with anti-GFP antibody from the proteins collected from the myocyte plates.

Statistical analysis. All the results are expressed as the mean $\pm$ standard error (SE) from three independent experiments. Data were analyzed using an independent-sample *t* test with SPSS software (version 14.0). For experiments with multiple comparisons, one-way analysis of variance (ANOVA) followed by Tukey's *post hoc* test was conducted. Results with *P* values of <0.05 were considered significant.

REFERENCES

1. Ho CY, López B, Coelho-Filho OR, Lakdawala NK, Cirino AL, Jarolim P, Kwong R, González A, Colan SD, Seidman JG, Díez J. 2010. Myocardial fibrosis as an early manifestation of hypertrophic cardiomyopathy. N Engl J Med 363:552–563. https://doi.org/10.1056/NEJMoa1002659.
2. Fan D, Takawale A, Lee J, Kassiri Z. 2012. Cardiac fibroblasts, fibrosis and extracellular matrix remodeling in heart disease. Fibrogenesis Tissue Repair 5:15. https://doi.org/10.1186/1755-1536-5-15.
3. Weber KT, Brilla CG. 1991. Pathological hypertrophy and cardiac interstitium. Fibrosis and renin-angiotensin-aldosterone system. Circulation 83:1849–1865.
4. Kong P, Christia P, Frangogiannis NG. 2014. The pathogenesis of cardiac fibrosis. Cell Mol Life Sci 71:549–574. https://doi.org/10.1007/s00018-013-1349-6.
5. Baker KM, Booz GW, Dostal DE. 1992. Cardiac actions of angiotensin II: role of an intracardiac renin-angiotensin system. Annu Rev Physiol 54:227–241. https://doi.org/10.1146/annurev.ph.54.030192.001303.
6. Hilfiker-Kleiner D, Landmesser U, Drexler H. 2006. Molecular mechanisms in heart failure: focus on cardiac hypertrophy, inflammation, angiogenesis, and apoptosis. J Am Coll Cardiol 48:A56–A66. https://doi.org/10.1016/j.jacc.2006.07.007.
7. Pathak M, Sarkar S, Vellaichamy E, Sen S. 2001. Role of myocytes in myocardial collagen production. Hypertension 37:833–840. https://doi.org/10.1161/01.HYP.37.3.833.
8. Sarkar S, Vellaichamy E, Young D, Sen S. 2004. Influence of cytokines and growth factors in ANG II-mediated collagen upregulation by fibroblasts in rats: role of myocytes. Am J Physiol Heart Circ Physiol 287:H107–H117. https://doi.org/10.1152/ajpheart.00763.2003.
9. Mir SA, Chatterjee A, Mitra A, Pathak K, Mahata SK, Sarkar S. 2012. Inhibition of signal transducer and activator of transcription 3 (STAT3) attenuates interleukin-6 (IL-6)-induced collagen synthesis and resultant hypertrophy in rat heart. J Biol Chem 287:2666–2677. https://doi.org/10.1074/jbc.M111.246173.
10. Willey CD, Palanisamy AP, Johnston RK, Mani SK, Shiraishi H, Tuxworth WJ, Zile MR, Balasubramanian S, Kuppuswamy D. 2008. STAT3 activation in pressure-overloaded feline myocardium: role for integrins and the tyrosine kinase BMX. Int J Biol Sci 4:184–199.
11. Fiaschi T, Magherini F, Gamberi T, Lucchese G, Faggian G, Modesti A, Modesti PA. 2014. Hyperglycemia and angiotensin II cooperate to enhance collagen I deposition by cardiac fibroblasts through a ROS-STAT3-dependent mechanism. Biochim Biophys Acta 1843:2603–2610. https://doi.org/10.1016/j.bbamcr.2014.07.009.
12. Haghikia A, Ricke-Hoch M, Stapel B, Gorst I, Hilfiker-Kleiner D. 2014. STAT3, a key regulator of cell-to-cell communication in the heart. Cardiovasc Res 102:281–289. https://doi.org/10.1093/cvr/cvu034.
13. Wang Y, van Boxel-Dezaire AH, Cheon H, Yang J, Stark GR. 2013. STAT3 activation in response to IL-6 is prolonged by the binding of IL-6 receptor to EGF receptor. Proc Natl Acad Sci U S A 110:16975–16980. https://doi.org/10.1073/pnas.1315862110.
14. Yun UJ, Park SE, Jo YS, Kim J, Shin DY. 2012. DNA damage induces the IL-6/STAT3 signaling pathway, which has anti-senescence and growth-promoting functions in human tumors. Cancer Lett 323:155–160. https://doi.org/10.1016/j.canlet.2012.04.003.
15. Niemand C, Nimmesgern A, Haan S, Fischer P, Schaper F, Rossaint R, Heinrich PC, Müller-Newen G. 2003. Activation of STAT3 by IL-6 and IL-10 in primary human macrophages is differentially modulated by suppressor of cytokine signaling 3. J Immunol 170:3263–3272. https://doi.org/10.4049/jimmunol.170.6.3263.
16. Marg A, Shan Y, Meyer T, Meissner T, Brandenburg M, Vinkemeier U. 2004. Nucleocytoplasmic shuttling by nucleoporins Nup153 and Nup214 and CRM1-dependent nuclear export control the subcellular distribution of latent Stat1. J Cell Biol 165:823–833. https://doi.org/10.1083/jcb.200403057.
17. Levy DE, Lee CK. 2002. What does Stat3 do? J Clin Invest 109:1143–1148. https://doi.org/10.1172/JCI0215650.

18. Yu H, Lee H, Herrmann A, Buettner R, Jove R. 2014. Revisiting STAT3 signalling in cancer: new and unexpected biological functions. Nat Rev Cancer 14:736–746. https://doi.org/10.1038/nrc3818.

19. Pranada AL, Metz S, Herrmann A, Heinrich PC, Müller-Newen G. 2004. Real time analysis of STAT3 nucleocytoplasmic shuttling. J Biol Chem 279:15114–15123. https://doi.org/10.1074/jbc.M312530200.

20. Ng IH, Bogoyevitch MA, Jans DA. 2014. Cytokine-induced slowing of STAT3 nuclear import; faster basal trafficking of the STAT3β isoform. Traffic 15:946–960. https://doi.org/10.1111/tra.12181.

21. Prinsloo E, Kramer AH, Edkins AL, Blatch GL. 2012. STAT3 interacts directly with Hsp90. IUBMB Life 64:266–273. https://doi.org/10.1002/iub.607.

22. Shah M, Patel K, Fried VA, Sehgal PB. 2002. Interactions of STAT3 with caveolin-1 and heat shock protein 90 in plasma membrane raft and cytosolic complexes: preservation of cytokine signaling during fever. J Biol Chem 277:45662–45669. https://doi.org/10.1074/jbc.M205935200.

23. Sato N, Yamamoto T, Sekine Y, Yumioka T, Junicho A, Fuse H, Matsuda T. 2003. Involvement of heat-shock protein 90 in the interleukin-6-mediated signaling pathway through STAT3. Biochem Biophys Res Commun 300:847–852. https://doi.org/10.1016/S0006-291X(02)02941-8.

24. Schoof N, von Bonin F, Trümper L, Kube D. 2009. HSP90 is essential for Jak-STAT signaling in classical Hodgkin lymphoma cells. Cell Commun Signal 7:17. https://doi.org/10.1186/1478-811X-7-17.

25. Kolosenko I, Grander D, Tamm KP. 2014. IL-6 activated JAK/STAT3 pathway and sensitivity to Hsp90 inhibitors in multiple myeloma. Curr Med Chem 21:3042–3047. https://doi.org/10.2174/0929867321666140414100831.

26. Datta R, Bansal T, Rana S, Datta K, Chattopadhyay S, Chawla-Sarkar M, Sarkar S. 2015. Hsp90/Cdc37 assembly modulates TGFβ receptor-II to act as a profibrotic regulator of TGFβ signaling during cardiac hypertrophy. Cell Signal 27:2410–2424. https://doi.org/10.1016/j.cellsig.2015.09.005.

27. Tomcik M, Zerr P, Pitkowski J, Palumbo-Zerr K, Avouac J, Distler O, Becvar R, Senolt L, Schett G, Distler JH. 2014. Heat shock protein 90 (Hsp90) inhibition targets canonical TGF-β signalling to prevent fibrosis. Ann Rheum Dis 73:1215–1222. https://doi.org/10.1136/annrheumdis-2012-203095.

28. Lee WJ, Lee JH, Ahn HM, Song SY, Kim YO, Lew DH, Yun CO. 2015. Heat shock protein 90 inhibitor decreases collagen synthesis of keloid fibroblasts and attenuates the extracellular matrix on the keloid spheroid model. Plast Reconstr Surg 136:328e–337e. https://doi.org/10.1097/PRS.0000000000001538.

29. Bellaye PS, Burgy O, Causse S, Garrido C, Bonniaud P. 2014. Heat shock proteins in fibrosis and wound healing: good or evil? Pharmacol Ther 143:119–132. https://doi.org/10.1016/j.pharmthera.2014.02.009.

30. Noh H, Kim HJ, Mi RY, Kim WY, Kim J, Ryu JH, Kwon SH, Jeon JS, Han DC, Ziyadeh F. 2012. Heat shock protein 90 inhibitor attenuates renal fibrosis through degradation of transforming growth factor-β type II receptor. Lab Invest 92:1583–1596. https://doi.org/10.1038/labinvest.2012.127.

31. Bang C, Batkai S, Dangwal S, Gupta SK, Foinquinos A, Holzmann A, Just A, Remke J, Zimmer K, Zeug A, Ponimaskin E. 2014. Cardiac fibroblast-derived microRNA passenger strand-enriched exosomes mediate cardiomyocyte hypertrophy. J Clin Invest 124:2136–2146. https://doi.org/10.1172/JCI70577.

32. Dai B, Cui M, Zhu M, Su WL, Qiu MC, Zhang H. 2013. STAT1/3 and ERK1/2 synergistically regulate cardiac fibrosis induced by high glucose. Cell Physiol Biochem 32:960–971. https://doi.org/10.1159/000354499.

33. Fredj S, Bescond J, Louault C, Delwail A, Lecron JC, Potreau D. 2005. Role of interleukin-6 in cardiomyocyte/cardiac fibroblast interactions during myocyte hypertrophy and fibroblast proliferation. J Cell Physiol 204:428–436. https://doi.org/10.1002/jcp.20307.

34. Ancey C, Corbi P, Froger J, Delwail A, Wijdenes J, Gascan H, Potreau D, Lecron JC. 2002. Secretion of IL-6, IL-11 and LIF by human cardiomyocytes in primary culture. Cytokine 18:199–205. https://doi.org/10.1006/cyto.2002.1033.

35. Libermann TA, Baltimore DA. 1990. Activation of interleukin-6 gene expression through the NF-kappa B transcription factor. Mol Cell Biol 10:2327–2334. https://doi.org/10.1128/MCB.10.5.2327.

36. Zhang YH, Lin JX, Vilcek J. 1990. Interleukin-6 induction by tumor necrosis factor and interleukin-1 in human fibroblasts involves activation of a nuclear factor binding to a kappa B-like sequence. Mol Cell Biol 10:3818–3823. https://doi.org/10.1128/MCB.10.7.3818.

37. Hungness ES, Luo GJ, Pritts TA, Sun X, Robb BW, Hershko D, Hasselgren PO. 2002. Transcription factors C/EBP-β and -δ regulate IL-6 production in IL-1β-stimulated human enterocytes. J Cell Physiol 192:64–70. https://doi.org/10.1002/jcp.10116.

38. Ray A, Sassone-Corsi P, Sehgal PB. 1989. A multiple cytokine-and second messenger-responsive element in the enhancer of the human interleukin-6 gene: similarities with c-fos gene regulation. Mol Cell Biol 9:5537–5547. https://doi.org/10.1128/MCB.9.12.5537.

39. Matsui H, Ihara Y, Fujio Y, Kunisada K, Akira S, Kishimoto T, Yamauchi-Takihara K. 1999. Induction of interleukin (IL)-6 by hypoxia is mediated by nuclear factor (NF)-κB and NF-IL6 in cardiac myocytes. Cardiovasc Res 42:104–112. https://doi.org/10.1016/S0008-6363(98)00285-5.

40. Stephanou A, Isenberg AD, Akira S, Kishimoto T, Latchman SD. 1998. The nuclear factor interleukin-6 (NF-IL6) and signal transducer and activator of transcription-3 (STAT-3) signalling pathways co-operate to mediate the activation of the hsp90β gene by interleukin-6 but have opposite effects on its inducibility by heat shock. Biochem J 330:189–195. https://doi.org/10.1042/bj3300189.

41. Chatterjee A, Mir SA, Dutta D, Mitra A, Pathak K, Sarkar S. 2011. Analysis of p53 and NF-κB signaling in modulating the cardiomyocyte fate during hypertrophy. J Cell Physiol 226:2543–2554. https://doi.org/10.1002/jcp.22599.

42. Hayden MS, Ghosh S. 2004. Signaling to NF-κB. Genes Dev 18:2195–2224. https://doi.org/10.1101/gad.1228704.

43. Broemer M, Krappmann D, Scheidereit C. 2004. Requirement of Hsp90 activity for IκB kinase (IKK) biosynthesis and for constitutive and inducible IKK and NF-κB activation. Oncogene 23:5378–5386. https://doi.org/10.1038/sj.onc.1207705.

44. Chen G, Cao P, Goeddel DV. 2002. TNF-induced recruitment and activation of the IKK complex require Cdc37 and Hsp90. Mol Cell 9:401–410. https://doi.org/10.1016/S1097-2765(02)00450-1.

45. Lee KH, Jang Y, Chung JH. 2010. Heat shock protein 90 regulates IκB kinase complex and NF-κB activation in angiotensin II-induced cardiac cell hypertrophy. Exp Mol Med 42:703–711. https://doi.org/10.3858/emm.2010.42.10.069.

46. Pratt WB, Toft DO. 2003. Regulation of signaling protein function and trafficking by the hsp90/hsp70-based chaperone machinery. Exp Biol Med 228:111–133. https://doi.org/10.1177/153537020322800201.

47. Eckl JM, Scherr MJ, Freiburger L, Daake MA, Sattler M, Richter K. 2015. Hsp90 · Cdc37 complexes with protein kinases form cooperatively with multiple distinct interaction sites. J Biol Chem 290:30843–30854. https://doi.org/10.1074/jbc.M115.693150.

48. Bretz NP, Ridinger J, Rupp AK, Rimbach K, Keller S, Rupp C, Marmé F, Umansky L, Umansky V, Eigenbrod T, Sammar M. 2013. Body fluid exosomes promote secretion of inflammatory cytokines in monocytic cells via Toll-like receptor signaling. J Biol Chem 288:36691–36702. https://doi.org/10.1074/jbc.M113.512806.

49. Tominaga N, Hagiwara K, Kosaka N, Honma K, Nakagama H, Ochiya T. 2014. RPN2-mediated glycosylation of tetraspanin CD63 regulates breast cancer cell malignancy. Mol Cancer 13:134. https://doi.org/10.1186/1476-4598-13-134.

50. Verweij FJ, Van Eijndhoven MA, Hopmans ES, Vendrig T, Wurdinger T, Cahir-McFarland E, Kieff E, Geerts D, van der Kant R, Neefjes J, Middeldorp JM. 2011. LMP1 association with CD63 in endosomes and secretion via exosomes limits constitutive NF-κB activation. EMBO J 30:2115–2129. https://doi.org/10.1038/emboj.2011.123.

51. Pols MS, Klumperman J. 2009. Trafficking and function of the tetraspanin CD63. Exp Cell Res 315:1584–1592. https://doi.org/10.1016/j.yexcr.2008.09.020.

52. Clayton A, Turkes A, Navabi H, Mason MD, Tabi Z. 2005. Induction of heat shock proteins in B-cell exosomes. J Cell Sci 118:3631–3638. https://doi.org/10.1242/jcs.02494.

53. Gupta S, Knowlton AA. 2007. HSP60 trafficking in adult cardiac myocytes: role of the exosomal pathway. Am J Physiol Heart Circ Physiol 292:H3052–H3056. https://doi.org/10.1152/ajpheart.01355.2006.

54. Chung SW, Lee JH, Choi KH, Park YC, Eo SK, Rhim BY, Kim K. 2009. Extracellular heat shock protein 90 induces interleukin-8 in vascular smooth muscle cells. Biochem Biophys Res Commun 378:444–449. https://doi.org/10.1016/j.bbrc.2008.11.063.

55. Essandoh K, Yang L, Wang X, Huang W, Qin D, Hao J, Wang Y, Zingarelli B, Peng T, Fan GC. 2015. Blockade of exosome generation with GW4869 dampens the sepsis-induced inflammation and cardiac dysfunction. Biochim Biophys Acta 1852:2362–2371. https://doi.org/10.1016/j.bbadis.2015.08.010.

56. Yu X, Deng L, Wang D, Li N, Chen X, Cheng X, Yuan J, Gao X, Liao M, Wang M, Liao Y. 2012. Mechanism of TNF-α autocrine effects in hypoxic cardiomyocytes: initiated by hypoxia inducible factor 1α, presented by

exosomes. J Mol Cell Cardiol 53:848–857. https://doi.org/10.1016/j.yjmcc.2012.10.002.

57. Lee KS, Park JH, Lee S, Lim HJ, Choi HE, Park HY. 2007. HB-EGF induces delayed STAT3 activation via NF-κB mediated IL-6 secretion in vascular smooth muscle cell. Biochim Biophys Acta 1773:1637–1644. https://doi.org/10.1016/j.bbamcr.2007.07.001.

58. National Institutes of Health. 1996. Institutional administrator's manual for laboratory animal care and use. NIH publication no. 85-23. National Institutes of Health, Bethesda, MD.

59. Sil P, Sen S. 1997. Angiotensin II and myocyte growth role of fibroblasts. Hypertension 30(2 Pt 1):209–216.

60. Rana S, Datta K, Reddy TL, Chatterjee E, Sen P, Pal-Bhadra M, Bhadra U, Pramanik A, Pramanik P, Chawla-Sarkar M, Sarkar S. 2015. A spatio-temporal cardiomyocyte targeted vector system for efficient delivery of therapeutic payloads to regress cardiac hypertrophy abating bystander effect. J Control Release 200:167–178. https://doi.org/10.1016/j.jconrel.2015.01.008.

61. Ray A, Rana S, Banerjee D, Mitra A, Datta R, Naskar S, Sarkar S. 2016. Improved bioavailability of targeted curcumin delivery efficiently regressed cardiac hypertrophy by modulating apoptotic load within cardiac microenvironment. Toxicol Appl Pharmacol 290:54–65. https://doi.org/10.1016/j.taap.2015.11.011.

62. Antrobus R, Borner GH. 2011. Improved elution conditions for native co-immunoprecipitation. PLoS One 6:e18218. https://doi.org/10.1371/journal.pone.0018218.

63. Savina A, Vidal M, Colombo MI. 2002. The exosome pathway in K562 cells is regulated by Rab11. J Cell Sci 115(Pt 12):2505–2515.

64. Savina A, Furlán M, Vidal M, Colombo MI. 2003. Exosome release is regulated by a calcium-dependent mechanism in K562 cells. J Biol Chem 278:20083–20090. https://doi.org/10.1074/jbc.M301642200.

65. Théry C, Amigorena S, Raposo G, Clayton A. 2006. Isolation and characterization of exosomes from cell culture supernatants and biological fluids. Curr Protoc Cell Biol Chapter 3:Unit 3.22. https://doi.org/10.1002/0471143030.cb0322s30.